DALHOUSIE UNIVERSITY

EXPERIMENTAL STUDY OF POSITIVE TRIGONS ON DIAMONDS; CONDITIONS OF NEAR-SURFACE DIAMOND RESORPTION WITH APPLICATION TO EMPLACEMENT CONDITIONS OF SNAP LAKE KIMBERLITE.

Njillan Forbes

SUBMITTED IN PARTIAL FULFILLMENT OF THE REQUIREMENTS
FOR THE BACHELOR OF SCIENCE, HONORS
DEPARTMENT OF EARTH SCIENCES
DALHOUSIE UNIVERSITY, HALIFAX, NOVA SCOTIA

March 2017

Distribution License

DalSpace requires agreement to this non-exclusive distribution license before your item can appear on DalSpace.

NON-EXCLUSIVE DISTRIBUTION LICENSE

You (the author(s) or copyright owner) grant to Dalhousie University the non-exclusive right to reproduce and distribute your submission worldwide in any medium.

You agree that Dalhousie University may, without changing the content, reformat the submission for the purpose of preservation.

You also agree that Dalhousie University may keep more than one copy of this submission for purposes of security, back-up and preservation.

You agree that the submission is your original work, and that you have the right to grant the rights contained in this license. You also agree that your submission does not, to the best of your knowledge, infringe upon anyone's copyright.

If the submission contains material for which you do not hold copyright, you agree that you have obtained the unrestricted permission of the copyright owner to grant Dalhousie University the rights required by this license, and that such third-party owned material is clearly identified and acknowledged within the text or content of the submission.

If the submission is based upon work that has been sponsored or supported by an agency or organization other than Dalhousie University, you assert that you have fulfilled any right of review or other obligations required by such contract or agreement.

Dalhousie University will clearly identify your name(s) as the author(s) or owner(s) of the submission, and will not make any alteration to the content of the files that you have submitted.

If you have questions regarding this license please contact the repository manager at dalspace@dal.ca.

Grant the distribution license by signing and dating below.

_____ _____

Name of signatory Date

DALHOUSIE UNIVERSITY

Department of Earth Sciences
Halifax, Nova Scotia
B3H 4R2
(902)- 494-2358

DATE: 28 April 2017

AUTHOR: **Njillan Forbes**

TITLE: ***Experimental study of positive trigons on diamonds; conditions of near-surface diamond resorption with application to emplacement conditions of Snap Lake kimberlite.***

Degree: B. Sc. Honours Earth Sciences Convocation: June Year: 2017

ABSTRACT

Kimberlites are volatile-rich ultrabasic igneous rocks and the primary source rock of diamonds. During ascent in kimberlite magmas and perhaps after emplacement, diamonds undergo resorption by interaction with kimberlitic fluids, yielding a variety of resorption features on diamonds including triangular etch pits (trigons). Positive trigons have been proposed to form as a result of diamond resorption in either oxidizing or reducing conditions depending on the kimberlite pressure, temperature and melt composition, and they are rare on natural diamonds compared pervasive negative trigons. Diamonds from Snap Lake kimberlite dyke in Northwest Territories, Canada have abundant positive trigons. The nature of fluids and emplacement conditions responsible for Snap Lake positive trigons are not well known. Published experimental studies indicate temperature and oxygen fugacity controls on trigon orientation and morphology, although the data is sparse. A better understanding of these controls can help to constrain the conditions that prevailed in kimberlites that host positive trigon-bearing diamonds.

This study focuses on experimental production of positive trigons under variable temperatures and oxygen fugacities, to observe and quantify changes in their morphology. I performed resorption experiments in Na_2CO_3-NaCl melt at 0.1 MPa (atmospheric pressure), temperatures 700 ºC and 800 ºC (to examine near surface emplacement conditions), and oxygen fugacity in air ($\log fO_2 = -0.68$) and in pure CO_2 ($\log fO_2 = -2.79$ and -2.85). Geometric parameters of positive trigons were examined by conducting quantitative measurements using an atomic force microscope. All except one of the experiments produced positive trigons. Comparison of the results to prior experimental studies of positive trigons confirms different evolution trends for point- and flat-bottomed positive trigons as temperature and oxygen fugacity increases. Comparison of the results to Snap Lake positive trigons helps better understand possible emplacement conditions of Snap Lake kimberlite.

Keywords: Snap Lake kimberlite, positive trigons, diamond resorption, trigon morphology, kimberlitic fluids, experimental petrology.

TABLE OF CONTENTS

LIST OF FIGURES

LIST OF TABLES

ACKNOWLEDGEMENTS

I would like to thank all the people who contributed in some way to this thesis. Firstly, I thank my supervisor, Professor Yana Fedortchouk, for accepting me into her group, supporting my attendance at the Atlantic Geoscience Society Conference 2017 and being available to guide me throughout this thesis. Next, I thank Professor Djordje Grujic for his open door to discuss my thesis and give helpful feedback. I would like to thank Professor James Brenan and his graduate student, Erin Keltie for assisting with experiments conducted in the gas-mixing furnace. I would like to thank my fellow lab mates who have supported this thesis in one way or another; Luke Hilchie for giving me helpful comments, Ryan Kressall for answering my questions and Zhuoyuan Li who helped with AFM work and allowed me to read and cite a bit of his unpublished data. I am grateful for the Slaight Family Foundation Scholarship that allowed me to pursue my undergraduate degree. Finally, I would like to acknowledge friends and family who supported me during my thesis. I want to thank Vicki Olatundun, Doretta Zinck, Yanna Conway, and Angela Forbes for their encouragement and prayers. I want to thank Eiblin Koch, Esther Schwarz, Farah Henry and Naa Torshie Obodai for their constant love and friendship. Lastly, I would like to thank my late mother, Dr. Lizbeth Forbes for always believing in me and inspiring me daily.

1. INTRODUCTION

1.1 Diamonds and Kimberlites: Origin and Composition

Diamonds form in regions with very low geothermal gradients, such as the subcratonic lithosphere with relatively low temperatures and high pressures. The subcratonic lithosphere can extend to depths > 250 km and due to their relatively low temperatures ~ 1000 -1300 °C and extreme thickness, they are the main locations of diamond formation in the Earth's mantle (Tappert and Tappert, 2011). At depths > 100 km, a small-degree of partial melting (<1%) of the anhydrous carbonated mantle (peridotite) occurs and produces carbonatitic liquid below the subcratonic lithosphere (Brey et al., 2008). This carbonatitic liquid permeates through the subcratonic lithosphere allowing diamonds to nucleate at temperatures 1000 - 1300 °C and pressures between > 4 GPa (Palyanov et al., 2014).

Kimberlites are a main source rock of diamonds. Kimberlitic magmas are caused by a small-degree of partial melting (<1%) of carbonatized Lherzolite in the deep mantle (Frezzotti and Touret, 2014). The magma ascends from depths ~ 250 km (> 8 GPa) through the subcratonic lithosphere and incorporates various minerals (xenocrysts) and rock fragments (xenoliths). Many of these xenoliths from the subcratonic lithosphere break once incorporated into the kimberlite magma and release their mineral components including diamonds (Tappert and Tappert, 2011). Upon reaching the Earth's surface, the high velocity (30 - 50 m/s) rising kimberlite magma loses its highly compressed mantle-derived volatiles, which causes an explosion ejecting a mixture of gas and entrained particles into the atmosphere at a speed of ~ 600 m/s (Wilson et al., 2007). As a result of kimberlite eruption the remnant deposits are characterized by porous, cone-shaped, volcanic pipe diatremes surrounded by a crater rim of breccia and pyroclastic deposits (Wilson et al., 2007).

Mitchell (1986) describes kimberlite rocks as volatile-rich ultrabasic igneous rocks with mantle-sourced rounded phenocrysts of olivine, phlogopite, magnesian ilmenite, pyrope and Cr-poor titanian pyrope set in a fine grained groundmass of second generation olivine and phlogopite together with calcite, serpentine, magnetite and apatite. The composition of the primary kimberlite magma is still uncertain. Some researchers suggest the primary magma to be carbonate silicate melts with high volatiles (Cl, H_2O and CO_2)

and MgO (~ 25–31 wt%), low SiO_2 (~ 26–30 wt%), Al_2O_3 and alkalis contents (Kopylova et al., 2007; Kamenetsky et al., 2009). Kamenetsky et al. (2012) suggests that the primary kimberlite magma corresponds to an alkalic anhydrous carbonatitic melt (SiO_2 ~ 5 wt%), which became enriched in silica due to the assimilation of mantle xenoliths. Most kimberlites originally had a lower SiO_2 content and as such may have been transitional between silicate and carbonate melts, which results in higher CO_2 solubilities (Brooker et al. 2011). Kimberlite rocks are heterogeneous and variable in appearance due to the high abundance of xenocrysts and xenoliths incorporated into the kimberlitic magma (Figure 1.1-1). Kimberlite provinces occur in the geologically most ancient parts of cratons that were formed in the Archean eon (2.5 bya) (Tappert and Tappert, 2011).

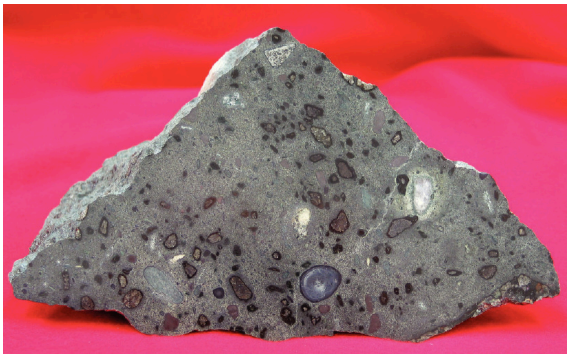

Figure 1.1-1 Hand sample of kimberlite rock from the Monastery mine, South Africa (Ø: ~25 cm), containing rounded and angular xenocrysts and xenoliths in a fine-grained matrix (Tappert and Tappert, 2011).

Kimberlitic magmatism was active in the recent time period from early Triassic to early Miocene (250 - 20 mya) during which most diamond-bearing kimberlites in Africa, North America, Australia, Asia, Europe and South America were emplaced (Tappert and Tappert, 2011) (Figure. 1.1-2).

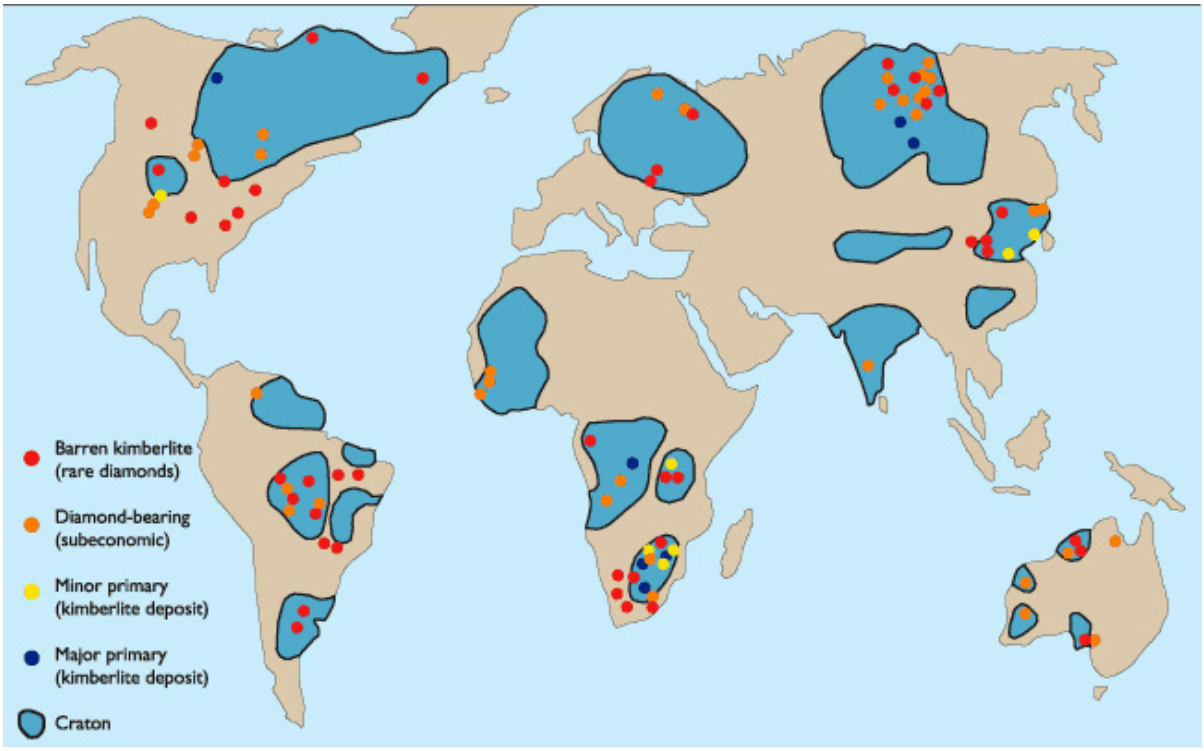

Figure 1.1-2 World map of craton and kimberlite distribution (Eckstrand et al., 1995).

1.2 Kimberlite pipe and dyke

Based on textural similarity of South African kimberlite sites, a classic kimberlite pipe model was developed consisting of three lithological facies (Dawson, 1971; Hawthorne, 1975; Mitchell, 1986): crater facies, diatreme facies and hypabyssal facies (Figure 1.2-1).

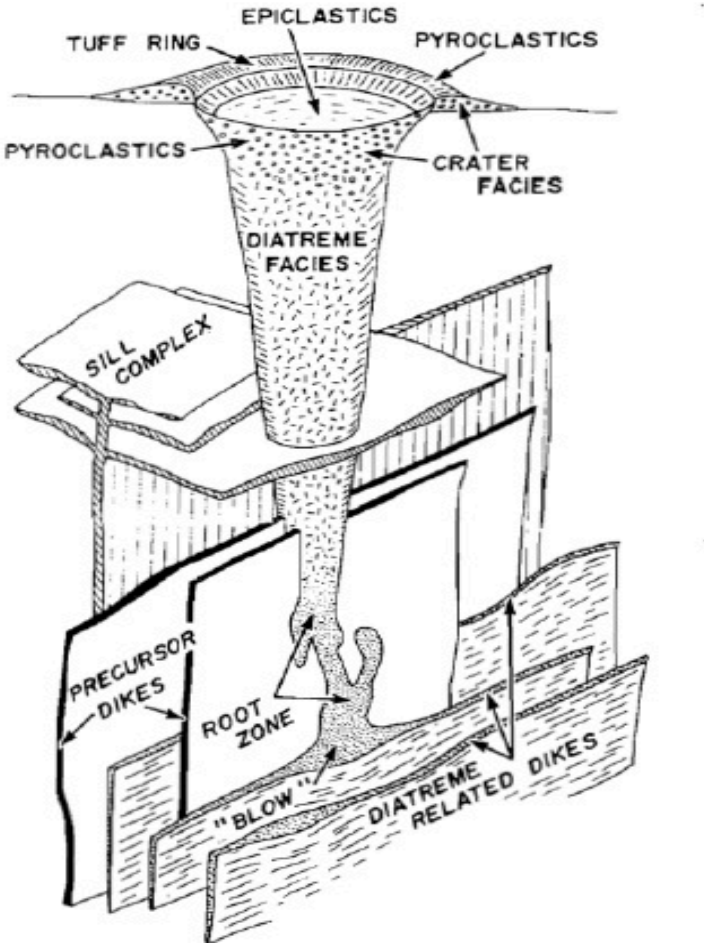

Figure 1.2-1 Classic kimberlite pipe model proposed by Mitchell (1986) based on example from southern Africa. Model showsg three lithological facies: crater facies, diatreme facies and hypabyssal facies.

However, Field and Smith (1999) showed that new kimberlite pipes discovered in Canada do not conform to the pipe models developed for South African kimberlites. This new discovery of diamond-bearing kimberlite deposits in Canada challenged the 'classic South African model' of a kimberlite pipe. New styles of kimberlite pipes identified in Canada include (Figure 1.2-2):

style 1- large shallow bowl-shaped pipes in filled largely with pyroclastic kimberlite (examples in Canadian Prairies),

style 2 - small steep-sided pipes in-filled primarily with re-sedimented volcaniclastic kimberlite (examples in Lac de Gras, Canada) and,

style 3 - small steep-sided pipes that contain tuffisitic breccia and hypabyssal kimberlite (examples in Gacho Kue, Northwestern Territories, Canada) (Field and Smith, 1999).

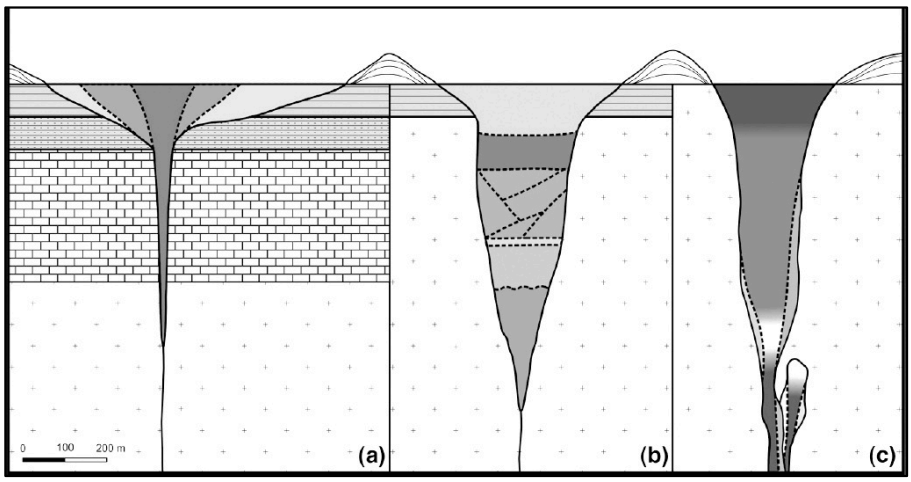

Figure 1.2-2 New styles of kimberlite pipes identified in Canada (a) Style 1 - large shallow bowl-shaped pipes, (b) Style 2 - small steep-sided pipes, (c) Style 3 - small steep-sided pipes similar to South Arfrican model pipes (Smith et al., 2008).

Different styles of kimberlite pipes can be largely impacted by the volatile composition of the kimberlite magma (Skinner et al., 2004). Moussallam et al. (2016) proposed that kimberlites can rise to depths of the upper crust (< 5 km) without suffering significant degassing and must release large quantities of volatiles (> 15 wt.%) within the very last few kilometers of ascent. This shallow degassing of kimberlites may explain the characteristic pipe morphology of widening-upward towards the crater from a ≤ 2.5 km deep root zone (Moussallam et al., 2016). H_2O-rich kimberlites produce strong CO_2 degassing at high pressure (depths ~ 2.6 km), resulting in pipes with deep root zones (style 2 and 3), whereas H_2O-poor kimberlites retain CO_2 up to shallow depths ~ 1.1 km at lower pressures, producing shallow root zones (Style 1) and promoting possible interaction with groundwater (Moussallam et al., 2016).

Kimberlite dikes also form from volatile-rich kimberlite magmas and commonly occur as swarms of parallel dikes (Mitchell, 1986) (Figure 1.2-1). Typically they are vertically dipping tabular bodies that are 1-3 m wide and are classified as hypabyssal kimberlites, which form at the root zones of kimberlite diatremes (Mitchell, 1986). Dikes occupy vertical to sub-vertical parallel fractures or joints of the country host rock, allowing their emplacement to be controlled by the regional fracture pattern (Mitchell, 1986). As a result of contact metamorphism during emplacement, dikes undergo

metasomatism producing alteration zones (Mitchell, 1986). Dikes can be traced along strike by the occurrence of such alteration zones or by the presence of fractures (Mitchell, 1986). Clement (1982) proposed that precursor dikes (Figure 1.2-1) represent an early pre-pipe episode of dike formation that penetrated to higher levels than the latter dikes, which have participated in diatreme and root zone formation. The emplacement of the precursor dikes may play an important role in diatreme localization and formation by providing zones of weakness and access points for groundwater into the magmatic system (Clement, 1982).

In summary, kimberlite pipes form from the root zones ~ 2.6 km towards the surface, and the different emplacement styles are controlled by volatile composition, which affects the depth of the root zones. On the contrary, kimberlite dikes form at the root zones showing distinct alteration zones, and the emplacement style is controlled by fractures in the host country rock.

1.3 Snap Lake Kimberlite Dike

Snap Lake dyke located in Northwest Territories, Canada is a Cambrian (523 Ma) complex segmented diamond-bearing hypabyssal kimberlite compromising a series of sub parallel sheets (Gernon et al., 2012) (Figure 1.3-1).

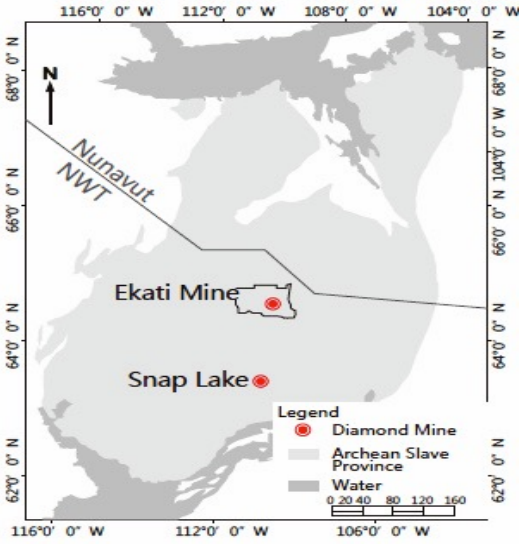

Figure 1.3-1. Map of Snap Lake and Ekati Diamond Mines in Northwestern Territories, Canada (Nowicki et al., 2004).

This dike measures 2 -3 m thick (Figure 1.3-2) and was emplaced onto low-porosity crystalline basement rocks (Gernon et al., 2012).

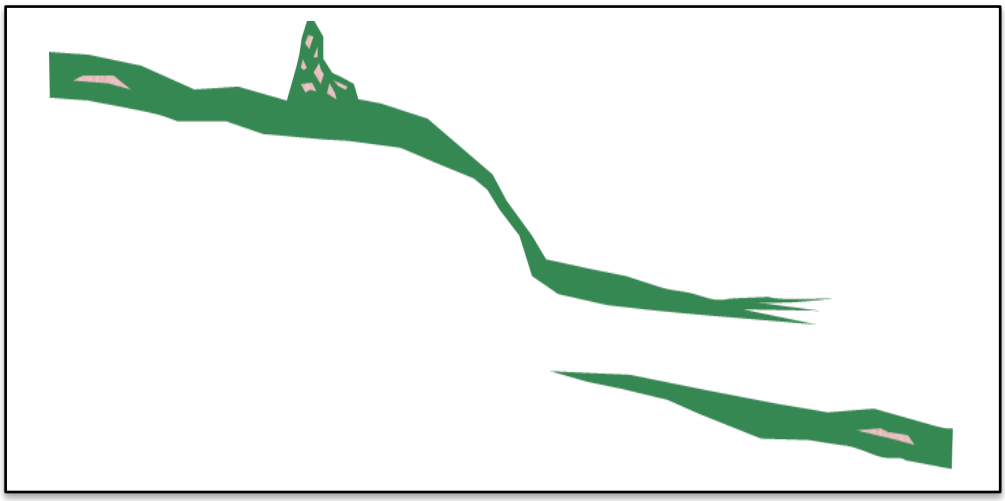

Figure 1.3-2 Snap Lake dike (DeBeers Report)

Snap Lake dike is strongly altered, and degrees and forms of alteration are explained by crustal contamination and secondary alteration (De Beers Internal Report). Petrographic studies of the Snap Lake intrusion by Gernon et al. (2012) suggest that the intrusion was multi-phase and emplaced by at least two magma batches. Gernon et al. (2012) proposed that the lack of grading and preservation of a sub vertical fabric within the Snap Lake intrusion suggests rapid degassing caused groundmass crystallization to occur rapidly during and after emplacement. Snap Lake dike is well exposed and fractures present in the crystalline basement rocks closely match the fractures of the Snap Lake dike, which infers that these may have influenced the kimberlite dike emplacement (Gernon et al., 2012).

Unlike most kimberlites including kimberlite pipes from Ekati mine also located in Northwest Territories, Snap Lake dike contains diamonds with abundant positive trigons (Li, 2015). Both Snap Lake and Ekati diamonds have similar morphologies of negative trigons present, however Ekati diamonds do not have the same abundance of positive trigons (Li, 2015). Li (unpublished data, February 2017) proposes that this unusual occurrence of abundant positive trigons on Snap Lake diamonds could be caused by a later resorption event of which the prevalent conditions are unknown.

1.4 Diamond Resorption as a Kimberlite Composition Proxy

Resorption morphology of kimberlitic diamonds is important for understanding the fluid systems and emplacement conditions of the host-kimberlite. Both growth and resorption features carry information about the media where these processes were occurring Zhang et al., 2011). During the ascent and at emplacement, oxidation occurs within the kimberlite magma resulting in partial resorption and etching of the hosted diamonds (Robinson, 1979). High temperature oxidation causing diamond resorption and etching commences approximately at 100 km and is completed by the time rising kimberlite magma reaches the root zone (~ 2.6 km) of the pipe (Robinson, 1979). Only a few diamonds undergo low temperature oxidation close to the Earth's surface (< 3 km) also causing diamond resorption and etching (Robinson, 1979), although the temperature limit of this kind of resorption is unknown. Diamond resorption surface features include trigonal etch pits (trigons), whose orientation (positive or negative) can be determined by temperature and oxygen fugacity (Yamaoka et al., 1980). Positive trigons are rare on natural kimberlitic diamonds, perhaps formed during low temperature oxidation (Robinson 1979). Although, Khokhryakov and Palyanov et al. (2010) conducted diamond resorption experiment at high pressures (5.7 – 7.0 GPa) and temperatures (1400 – 1750 °C) in CO_2- and H_2O-rich melts which produced positive trigons.

Many diamond resorption experimental studies were conducted at pressures > 1 GPa to constrain fluid composition and crystallization conditions of diamond-bearing kimberlite magma during their ascent. However, studies of diamond resorption conditions at pressures corresponding to near the Earth's surface (< 3 km) during kimberlite emplacement are few, and thus the potential extent of resorption under these conditions in nature are not well known.

1.5 Objectives and Approach of Experimental Study

Circulation of magmatic and meteoric fluids in kimberlite bodies is a controversial topic bearing on their primary chemical composition and petrogenesis, primary and secondary crystallization history, and cooling history. Understanding the controls of magmatic vs. meteoric fluid interaction on diamond resorption can be useful for understanding cooling and fluid-circulation history of kimberlites during emplacement. This study uses a new

approach by Fedortchouk et al. (2015) of examining the evolution of trigon pit morphology on diamonds using an Atomic Force Microscope (AFM), to understand the conditions of diamond residence in kimberlites.

To imitate near-surface diamond resorption, I describe resorption experiments in Na_2CO_3-NaCl melts at atmospheric pressure (0.1 MPa), at temperatures of 700 ºC and 800 ºC, and in two atmospheres (air and CO_2) to control oxygen fugacity. I present quantitative AFM results on the morphology of positive trigons, with implications for:
(1) better understanding the controls of temperature and oxygen fugacity on positive trigon development to further constrain the conditions of near-surface (< 3 km) diamond resorption, and the extent of resorption that can happen during kimberlite emplacement,
(2) constraining the individual effects of temperature and oxygen fugacity on positive trigon morphology to understand the controls of magmatic vs. meteoric fluid interaction on diamond resorption morphology during kimberlite cooling,
(3) constraining the emplacement conditions and nature of fluids that interacted with Snap Lake diamonds to produce abundant positive trigons - comparison to Li's (2015) study.

2. DIAMOND RESORPTION MORPHOLOGY

2.1 General Diamond Morphology

Many studies on diamond morphology conclude that octahedral or cubic diamonds are typical of kimberlites (Robinson, 1979). Tappert and Tappert (2011) distinguish three principle types of diamonds based on differences in morphology and growth mechanisms (Figure 2.1-1):

(1) monocrystalline diamonds consist of single diamond crystals,

(2) fibrous diamonds consist of elongated fibers,

(3) polycrystalline diamonds consist of numerous small diamond crystallites.

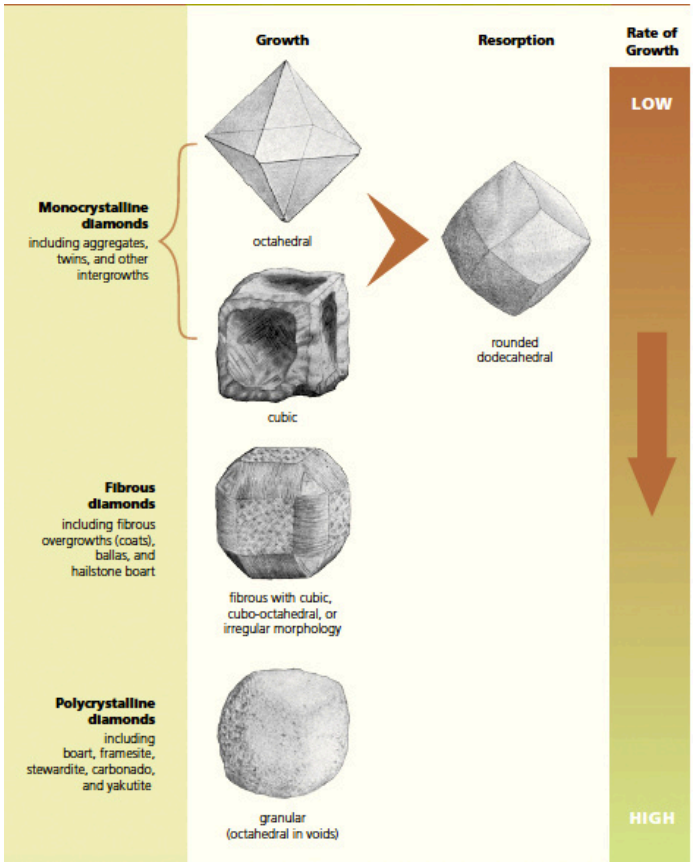

Figure 2.1-1. Tappert and Tappert (2011) Classification of three groups of diamonds based on morphological characteristics and growth mechanisms.

Most of the naturally occurring monocrystalline diamonds occur in three basic geometric forms: the octahedrons, cubes, or rhombic dodecahedrons. The dodecahedral habit results from resorption (Tappert and Tappert, 2011). The octahedral crystal shape is the only common natural diamond crystal shape and is generally accompanied with planar surfaces (Robinson, 1979). Octahedral shaped diamond crystals are indicative of slow growth rates under relatively stable conditions (Tappert and Tappert, 2011). Very few natural diamonds exhibit the ideal octahedron shape. Instead, most natural diamonds are distorted as a result of one growth direction favored over another (Tappert and Tappert, 2011). Incipient resorption of an octahedral diamond expresses as rounding of pointed corners, where surface area is highest (Tappert and Tappert, 2011). Resorption continues until the entire octahedral crystal faces dissolve resulting in a rounded dodecahedral habit (Tappert and Tappert, 2011). Figure 2.1-2 shows the transition from an octahedral to a dodecahedral diamond crystal habit and the subsequent loss of the original volume.

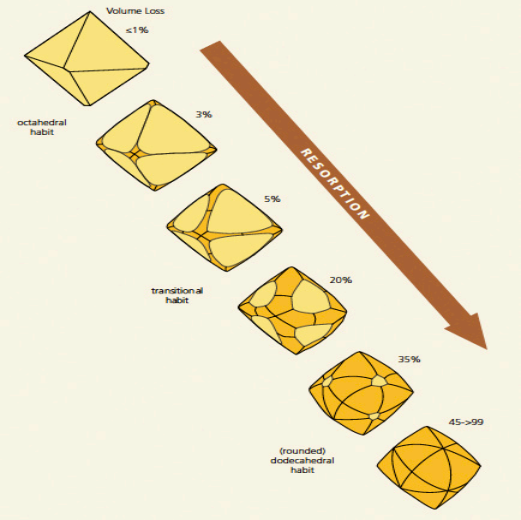

Figure 2.1-2 The stages of diamond resorption from octahedral to dodecahedral habit with respective volume loss Modified image from McCallum et al. (1994) by Tappert and Tappert (2011).

Two factors influence the habit of a dodecahedral diamond: the original growth habit and the extent of resorption (Tappert and Tappert, 2011). The ideal dodecahedral crystal consists of twelve equally sized rhombic faces, however, the faces of dodecahedral natural diamonds are always convex, which causes the dodecahedral diamond to appear rounded (Tappert and Tappert, 2011).

2.2 General Diamond Resorption Morphology

Diamond crystal surface textures can either be linked to growth in the mantle, or resorption in the kimberlite magma. Diamond resorption can be kimberlite-induced or mantle-derived, but this study will focus on kimberlite-induced resorption. Resorption processes that etch natural diamond surfaces include oxidation (Robinson, 1979). Most of the resorption surface textures are restricted to octahedral, cubic and dodecahedral crystal faces (Tappert and Tappert, 2011). Resorption surface textures on octahedral crystal faces include; triangular plates, shield-shaped laminae, triangular etch pits (trigons) and six-sided pits (Tappert and Tappert, 2011). Triangular plates are growth terraces of variable thickness that form on the crystal face and likely to represent separately nucleated octahedral overgrowths (Robinson, 1979). Triangular etch pits commonly known as trigons, are equilateral triangular pits, and are one of the most common features on natural diamond crystals (Robinson, 1979). Trigons can be variable in size at microscopic scales, and can be distinguished from one another by the shape of the pit-bottom (flat, point and round). Trigons on natural diamonds are commonly negatively oriented (oriented opposite to the underlying crystal {111} face) and rarely positively oriented (oriented identical to the underlying crystal {111} face) (Figure 2.2-1). Temperatures > 950 ºC and magmatic fluids are required to produce negative trigons (Robinson, 1979), which indicate negative trigons are dominantly early features during ascent. Positive trigons are much less common on natural diamonds than negative trigons, and are relatively late features (Robinson, 1979).

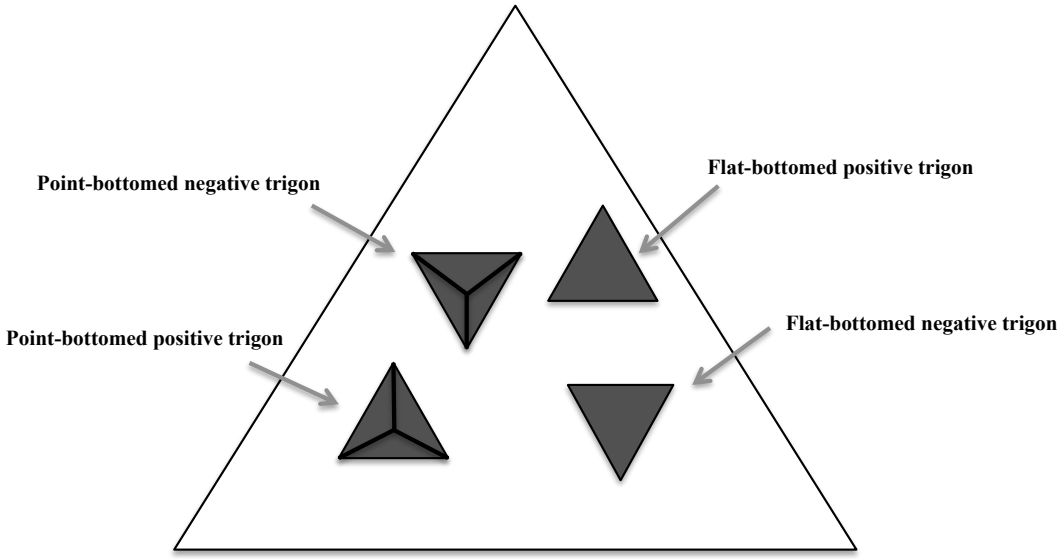

Figure 2.2-1 Schematic diagram of point- and flat-bottomed positive and negative trigons on an octahedral diamond {111} crystal face.

2.3 Resorption Morphology of Natural Kimberlitic Diamonds

Robinson (1979) studied natural diamonds from various kimberlite pipes and dykes and distinguished 41 pristine diamond surface textures, which he ascribed to mainly to resorption. Resorption morphology included; trigon pits, hexagonal pits containing trigon pits, serrate laminae, triangular plates, hillocks with hexagonal pits and fine striations (Robinson, 1979). Robinson (1979) recognized that certain etch features are restricted to particular crystallographic surfaces of diamond such as, trigonal pits to octahedral crystal surfaces and tetragonal pits to cubic crystal surfaces.

Gurney et al. (2004) presented a descriptive study of over 30,000 diamonds from thirteen host-kimberlites in Ekati diamond mine, Northwestern Territories, Canada (Figure 2.3-1).

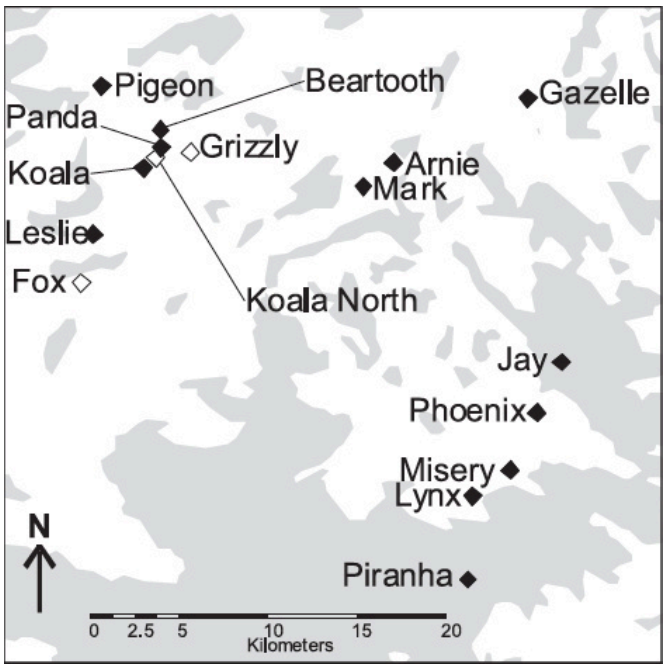

Figure 2.3-1 Map depicting relative geographic location of kimberlite localities in Ekati diamond mine (Gurney et al., 2004).

Gurney et al. (2004) groups the kimberlite localities based on broadly similar diamond population characteristics and on their geographic location:

(1) Koala, Panda, Beartooth, Pigeon and Leslie diamonds located Northwest, fall into a related group dominated by relatively unresorbed colorless and light brown octahedral diamonds in the large size fraction with fairly abundant cubes in the smaller sizes only,

(2) Jay, Phoenix, Misery, Lynx and Piranha located Southeast, fall into a group dominated by brown dodecahedral diamonds,

(3) Gazelle group located East of Panda and north of Misery is dominated by colorless and yellow dodecahedra diamonds, but has 35% octahedron, 3.6% cubes, and 6.3% aggregate diamonds,

(4) Arnie and Mark located East of Panda and West of Misery fall into a group dominated by fibrous cubic diamonds and very small proportions of flat-faced, step-faced, colorless, yellow and brown octahedral diamonds, colorless, yellow and brown dodecahedra and aggregate diamonds.

In summary, the range of resorption morphology that exists on populations of diamonds from different kimberlites within close geographic locations can vary substantially, and geographically related emplaced kimberlites can have significantly

different diamond populations.

2.4 Overview of Diamond Resorption Experiments

Diamond resorption morphology has been used in many experimental studies to investigate fluid compositions and conditions of crystallization of kimberlites. Experimental studies on the mechanism and kinetics of diamond resorption (Fedortchouk and Canil et al., 2009; Kozai and Arima et al., 2005) suggest that diamond resorption occurs as a result of an oxidation process, which involves breaking C-C bonds in the diamond crystal lattice to form CO or CO_2. More recent experimental studies (Khokhryakov and Palyanov et al., 2010; Fedortchouk et al., 2015) focus on the morphology of etched resorption features and their relationship with fluid or melt characteristics in the kimberlite magma.

Khokhryakov and Palyanov et al. (2010) investigated the influence of CO_2 and H_2O on diamond resorption morphology in carbonate melts as typically H_2O and CO_2 are regarded as diamond oxidizers in natural processes (Fedortchouk et al., 2007). Resorption experiments ran at a pressure range of 5.7–7.0 GPa, temperatures 1400 –1750 °C in fluid-free, CO_2-bearing and H_2O-bearing carbonate melts (Khokhryakov and Palyanov et al., 2010). These experiments imitate conditions of formation of kimberlite magma and the initial stages of magma ascent. H_2O-bearing carbonate and fluid-free melts both produced point-bottomed positive trigons, and CO_2-bearing carbonate melts produced numerous flat- and point-bottomed positive trigons (Khokhryakov and Palyanov et al., 2010). An increase (> 8 wt%) in H_2O content in carbonate melts produced negative trigons (Khokhryakov and Palyanov et al., 2010), so a relationship can be established between changes in the kimberlite magma H_2O content and the orientation of trigons. An evolution scheme for the morphology of octahedral diamond crystals during resorption in carbonate melts in depicted in Figure 2.4-1.

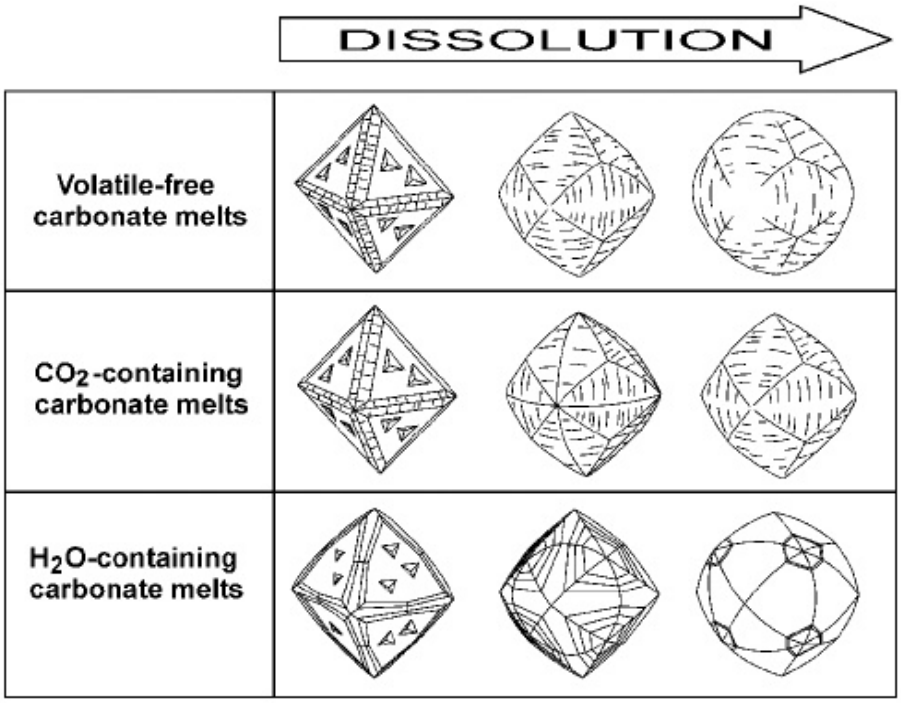

Figure 2.4-1 The evolution scheme for the morphology of octahedral diamond crystals during dissolution in carbonate melts (Khokhryakov and Palyanov et al., 2010).

Fedortchouk et al. (2015) conducted resorption experiments using 6 natural diamonds (octahedron crystals with minor pre-existing resorption features) from kimberlites in Ekati Mine, Canada and Yakutia, Russia. Experiments ran at 1 GPa, temperatures 1150 –1350 °C in the presence of H_2O-rich and CO_2 -rich melts. Experimentally produced etched pits were studied with an atomic force microscope (AFM). Overall experimental results show that resorption in CO_2-rich melt produced severe etching of pointed-bottomed positive and negative trigons and hexagonal pits, whereas, H_2O-rich melt produced only flat-bottomed negative trigons (Fedortchouk et al., 2015). CO_2 -rich melt produced positive trigons with diameters showing a strong positive correlation with the depth, and H_2O-rich melt produced trigons with diameters showing a weak correlation with depth (Fedortchouk et al., 2015). Fedortchouk et al. (2015) concludes that melt composition of kimberlites during resorption can affect the orientation and depth and diameter correlation of trigons.

Fedortchouk and Canil (2009) investigated diamond resorption at pressures corresponding to near surface diamond resorption to constrain the relationship between oxygen fugacity, temperature and other parameters that determine the morphology and

character of diamond surface features. Resorption experiments ran cut cubes of diamonds at 0.1 MPa, varying temperatures (1000, 1050 and 1100 °C) and oxygen fugacities (log fO_2 = 2 - 16.1) (Fedortchouk and Canil, 2009). Experimental results show that all diamonds developed on their {100} faces, large negative tetragons, positive tetragons and positive tetragons with a smaller negative tetragon on the inside (Fedortchouk and Canil et al., 2009). The tetragonal etch-pits started with a positive orientation at lower temperatures and high oxygen fugacities, and gradually became negative at higher temperatures and lower oxygen fugacities (Fedortchouk and Canil et al., 2009).

From the above-mentioned experimental studies, it can be concluded that a decrease in H_2O content in kimberlite melt, relatively lower temperatures and more oxidized conditions during oxidation will favor positive trigon orientation. However, the experimental grid corresponding to these variables and their effect on trigon orientation and morphology is poorly populated. Therefore, confident interpretation of the conditions of formation of natural positive trigons is vague in the absence of further experimentation.

2.5 Positive Trigons development on Kimberlitic Diamonds

Early studies (Fersman and Goldschmidt, 1911) proposed that O_2 gas and oxidizing fluids attack octahedral diamonds to produce positive trigons at temperatures < 950 °C. Robinson (1979) proposed that a strongly oxidizing environment at temperatures slightly above 1000 °C produce positive trigons. Positively oriented surface textures are mostly late features since they are produced at lower temperatures < 950 °C and at depths < 10 km (Robinson, 1979). Although, Khokhryakov and Palyanov et al. (2010) show that positively oriented trigons can also be etched at 5.7-7 GPa at depths > 10 km in CO_2-rich melts (reduced magmatic fluids).

Yamaoka (1980) examined the effects of temperature and oxygen fugacity on trigon orientation by placing natural octahedral diamond crystals in an oxide mixture (Fe-O and Mn-O) at 800 -1400 °C and 1.5 GPa. Experimental results show that a boundary curve exists at about 1000 °C separating positively from negatively oriented trigon formation (Yamaoka et al., 1980). The reversal of trigon orientation is caused by a change in the relative step velocities in the diamond crystal lattice; step 1 consists of triple-bonded

carbon atoms and step 2 are doubly bonded (Yamaoka et al., 1980). Figure 2.5-1 shows an octahedral diamond crystal face with step 1 and step 2. Relative step velocities are determined by the relative stabilities of the different oxygen-carbon bridges formed at both steps (Yamaoka et al., 1980). Therefore, at temperatures < 1000 °C the oxygen-carbon bridges at step 1 are not stabilized and have a faster velocity resulting in positive trigon formation (Yamaoka et al., 1980).

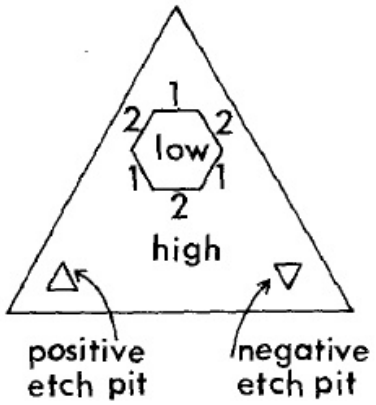

Figure 2.5-1 Step 1 and Step 2 on octahedral diamond face (Yamaoka et al., 1980).

Mathematical model developed by Angus and Dyble (1975) shows that dissolution etching favors a triangular shape due to the preferential removal of two-bonded carbon atoms rather than three- and four-bonded carbon atoms on the crystal face {111}. Positive trigon etch pits are less energetically favorable than negative ones because the removal of three-bonded carbon atoms is required to form positive trigons (Angus and Dyble, 1975). A schematic diagram (Figure. 2.5-2) shows the octahedral diamond crystal lattice of face {111} consisting of alternating rows of carbon atoms (row X and row O). The edges of positive trigons are defined by the removal of carbon atoms bound to the layer below, whereas, negative trigons are defined by the removal of carbon atoms not bound to the layer below (Angus and Dyble, 1975).

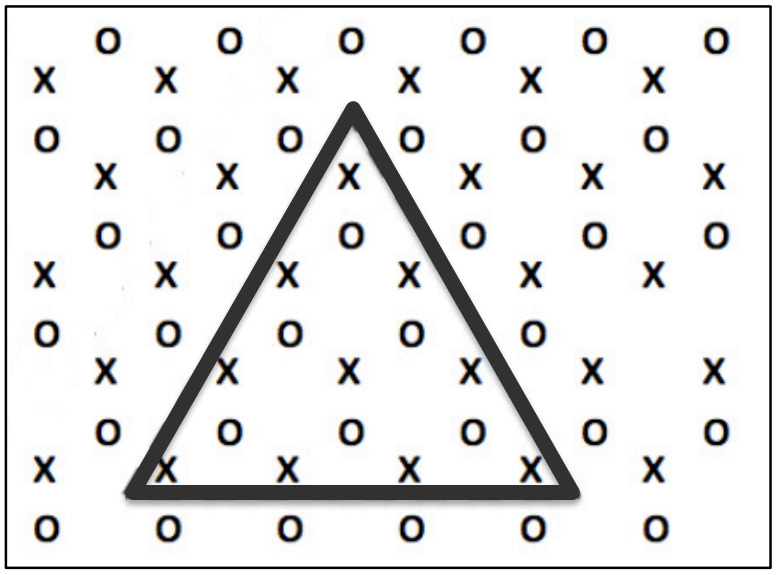

Figure 2.5-2 Schematic diagram of a portion of the top layer of alternating rows of carbon atoms (X and O) on the {111}-crystal face showing the removal of carbon atoms to produce a positive trigon (adapted from Angus and Dyble, 1975).

In summary, diamond resorption in strong oxidizing conditions at depths < 10 km and temperatures < 950 °C will produce positive trigons due to the faster velocity of step 1 compared to step 2 allowing the removal of three-bonded carbons. Although, kimberlite melt composition does have a control on positive trigon formation.

Keltie et al. (2016) examined how the presence of halogens in carbonate melts affects the morphology of positive trigons. Experiments exposed diamond crystals to melts of Na_2CO_3, Na_2CO_3-NaCl, and Na_2CO_3-NaF at 950ºC at atmospheric pressure (0.1 MPa) (Keltie et al., 2016). Experiments in Na_2CO_3-NaCl melt produced predominantly flat-bottomed and minor point-bottomed positive trigons with Y-, V-, and U-shaped walls on the {111} crystal face (Keltie et al., 2016). Keltie et al. (2016) confirmed that halogen presence in kimberlite melt affects the character of diamond resorption at atmospheric pressure favoring positive trigon formation. Rudenko et al. (1967) proposed that the presence of Cl in kimberlite melt alters the HCO complexes, and the strong electronegativity of Cl destabilizes the carbon-carbon bonds in the diamond crystal lattice making it easier for the removal of carbon atoms and diamond etching during resorption.

The above-mentioned experimental studies suggest that positive trigons form at temperatures < 950 °C in oxidizing conditions and at temperatures slightly above 1000°C in strongly oxidizing conditions. CO_2-rich (H_2O-poor) as well as Cl-rich carbonate

kimberlite melts also favor positive trigon formation. Therefore, conditions favoring positive trigon formation during resorption include, relatively low temperatures, oxidizing conditions and CO_2- and Cl-rich kimberlite melts. However, the extents to which these conditions control positive trigon formation have not been fully constrained; temperature limit and oxygen fugacity limit. In nature positive trigons on diamonds can form during resorption either as a result of interaction with meteoric fluids (oxidizing) near the surface, or magmatic fluids (reducing) at depth. This study aims to further contribute to the knowledge available of positive trigon formation by examining the individual controls of relatively lower temperatures (700 °C and 800 °C) and oxygen fugacities (air and in pure CO_2) in Cl-rich carbonate melt.

3. SAMPLES AND METHODS

3.1 Diamond Experimental Samples

Resorption experiments were conducted using 4 white octahedral diamond crystals with minimal surface features from a diamond mine in Yakutia, Russia. Table 3.1 lists detailed descriptions of each diamond sample. Microphotographs and Atomic Force Microscope (AFM) scans were taken on one crystal face of each of these diamonds before the experiments to ensure accurate recognition of the experimentally produced surface features.

Table 3.1 Description of diamond samples for dissolution experiments.

Sample	NF2	NF3	NF4	NF5
Crystal shape	Octahedral	Octahedral	Octahedral	Octahedral
Color	White	White	White	White
Weight (mg)	0.95	1.24	1.5	1.33
Growth features	None	None	Triangular plate	None
Resorption features	Shield-shaped laminae	Few large negative trigons	Few small negative & positive trigons	Few large negative trigons

3.2 Experimental Methods

The four diamond crystals were weighed then microphotographs were taken of each crystal face of each diamond with a petrographic microscope in reflected light. Each diamond was cleaned in a mixture H_2SO_4 and HNO_3 acids (5:3 volume ratio) boiling at 350 °C to remove any graphite on the crystal surfaces followed by an ethanol rinse. A mixture of powders of reagent grade Na_2CO_3 and NaCl (45:55 mol %) was used as the melt composition. The melt compositions were chosen to ensure that the dissolution conditions were above the liquidus for the Na_2CO_3-NaCl system (Figure 3.2-1).

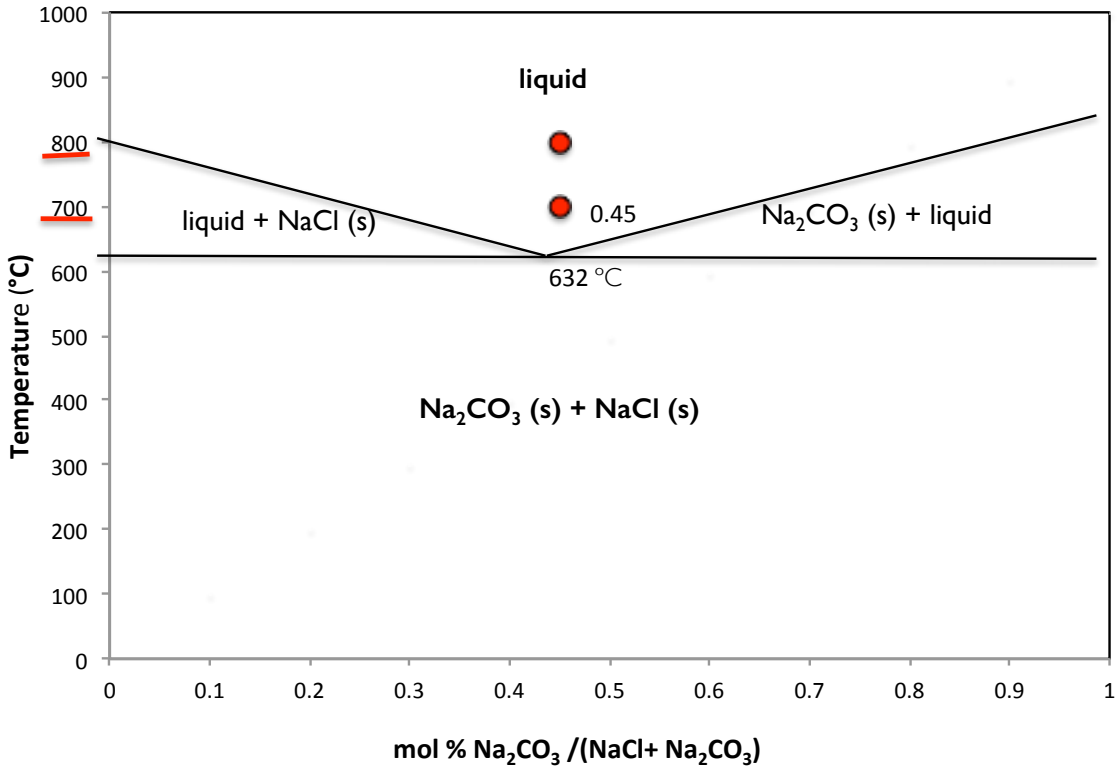

Figure 3.2-1 Phase diagram of Na_2CO_3-NaCl system with red dots showing experimental temperatures.

The diamonds were placed on the bottom of a 25 mL Al_2O_3 crucible weighing 35.46 g with the selected crystal face facing up to ensure direct interaction with the melt. The crucible was then filled with 5 g of the melt composition mixture for box furnace experiments and 2.2 g for gas-mixing experiments (Figure 3.2-2). The resorption experiments were conducted in a Ney Vulcan 3-550 box furnace for experimental runs air, and in a vertical tube gas-mixing furnace for runs in pure CO_2 (fO_2 log = -2.79 and -2.85).

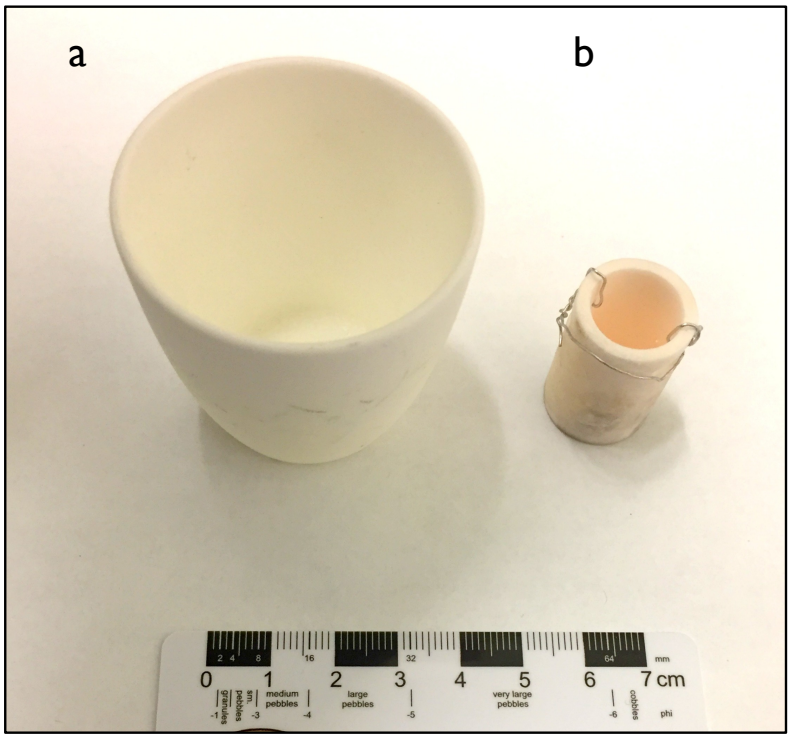

Figure 3.2-2 Al_2O_3 crucible for experiment in box furnace (a) and gas-mixing furnace (b).

Table 3.2-1 lists the diamond samples and the corresponding experimental conditions.

Sample	Run	T	Log	Duration
		°C	fO_2	(hr)
NF-2	1	700	-0.68	2.5
NF-2	2	700	-0.68	3
NF-3	1	800	-0.68	2.5
NF-3	2	800	-0.68	3
NF-4	1	800	-2.79	3
NF-5	1	700	-2.85	3.5

Table 3.2-2 lists the diamond sample with initial and final weight.

Sample	Initial weight (mg)	Final weight (mg)
NF-2	1.06	1.04
NF-3	1.24	1.22
NF-4	1.50	1.49
NF-5	1.33	1.33

After each experimental run, the diamond were extracted from the Na_2CO_3-NaCl melt using diluted HCl to dissolve the melt, then the diamonds were cleaned in the acid bath, micro-photographed and studied with the AFM. The AFM scans after each run provided a way to map the consequent evolution of the surface of the selected crystal faces. Experiments produced a large population of small positive trigons and grooves of positive trigons. After second runs the crystal face on diamonds became very rough therefore limiting the number of AFM scans that could be done on positive trigons.

3.2.1 Atomic Force Microscope

Atomic Force microscopy utilizes a sharp probe that scans across a surface of a sample monitoring the interaction between the probe and sample. The attraction and repulsion of atoms produces an interatomic force (van der Waals force) between the tip and sample surface causing the cantilever to bend or deflect during scanning. A detector measures the cantilever deflections using an optical technique involving a laser beam bouncing off the back of the deflecting cantilever onto a position-sensitive photo-detector (PSPD) which can measure displacements of light, and therefore, detect sub-angstrom vertical deflection of the cantilever tip (Howland and Benatar, 2000). The cantilever deflections measured

are processed by a computer, which generates a map of the surface topography. Figure 3.2.1-1 shows a schematic diagram of the AFM with the laser beam-bounce detection scheme.

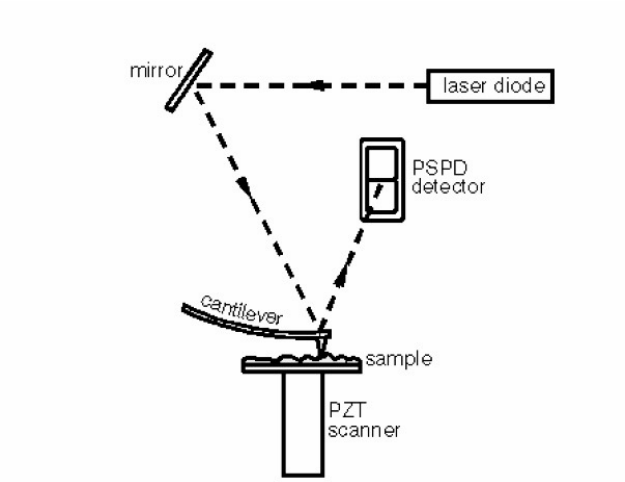

Figure 3.2.1-1 A schematic diagram of an AFM with cantilever deflection detected by a position-sensitive photo-detector (PSPD) through the laser beam-bounce detection scheme. (Howland and Benatar, 2000).

3.2.2 Study of Positive Trigons using AFM

Dalhousie University's Bruker MultiForce 8 Atomic Force Microscope was used to produce AFM scans of diamond surface resorption features. A silicon nitride probe was used with a spring constant of 0.1-0.6 N/m, a resonant frequency of 45-95 kHz, a nominal tip radius of curvature of 2 nm, and a length of 115 μm. Diamond samples with deep surface features were scanned at low rates (0.1 Hz) and scan maps were fit to a horizontal plane. AFM scan maps were processed using NanoScope software (8.10.) to measure the diameter, depth, wall slope angle, and wall shape of the trigons. Scan maps range in size from 100um^2 to 20 um^2. Larger scan sizes were used to examine shallow larger trigons and smaller scan sizes for deeper smaller trigons. Uncertainties in the data may arise from four sources:

(1) uncertainty inbuilt into the AFM (e.g. selection of measurement points on the diamond face),

(2) the accuracy of the AFM bearings (x, y, and z direction is +/- 1.4%), which is taken care of by regular calibration,

(3) selection of measurement points on cross section profiles is subjective and introduces

an uncertainty of +/- 1%,

(4) after the scan map is fitted to a horizontal plane, it may still dip at a small angle (< 1 º) relative to horizontal, which causes an uncertainty of +/- 0.2º in angle measurements. The total uncertainty for distance measurements was +/- 2.4% and for angle measurements +/- 0.2º (Zhang et al., 2015).

3.2.3 Gas-Mixing Furnace

At atmospheric pressures and high temperatures, gaseous buffering or gas mixing is the most common method used to control the oxygen fugacity, which is computed from the mixing ratios of the gases and the temperature by assuming equilibrium among the gaseous species (Darken and Gurry, 1945). Figure 3.2.3-1 is a schematic diagram showing the gas-mixing apparatus which involves purified gas passing through two flowmeters F_1 and F_2, consisting of capillary tubes C and manometer G containing butyl phthalate (Darken and Gurry, 1945). The drop in pressure in each flowmeter is kept constant by bleeding out through other tubes B, held at fixed levels in a water tank W (Darken and Gurry, 1945).

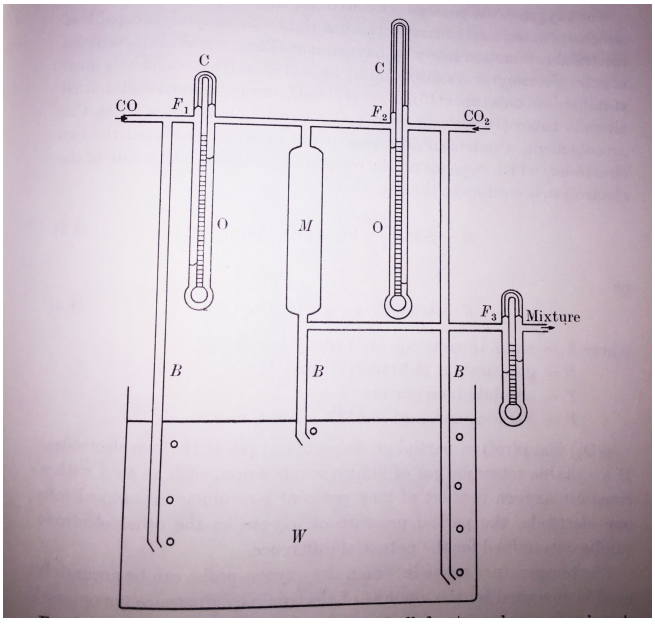

Figure 3.2-3-1 A schematic diagram of gas-mixing apparatus with two flowmeters F_1 and F_2, capillary tubes C, manometer G, water tank W and other tubes B (Darken and Gurry, 1945).

Dalhousie University's vertical tube gas-mixing furnace was used to conduct oxygen fugacity controlled experiments. A mixture of CO_2-CO gases was used for controlling oxygen fugacity. Controlling oxygen fugacity using this gas-mixing method involves careful calibration of both the flowmeters and final gas mixtures (Edgar, 1973). A zirconia sensor was used to measure the oxygen fugacity in the furnace.

4. EXPERIMENTAL RESULTS

4.1 Experiments at 700 °C in Air

Initial

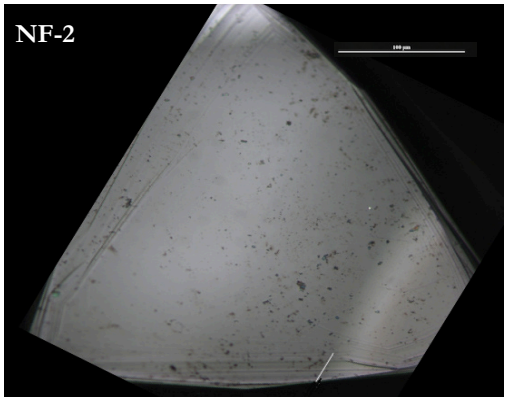

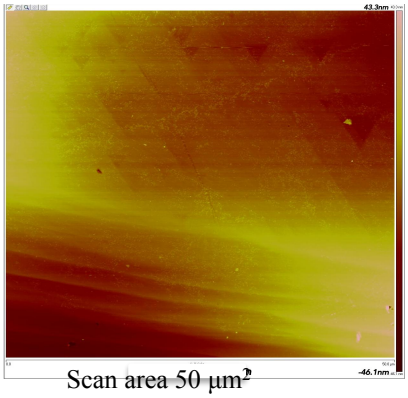

Scan area 50 μm²

In Air for 2.5 hours

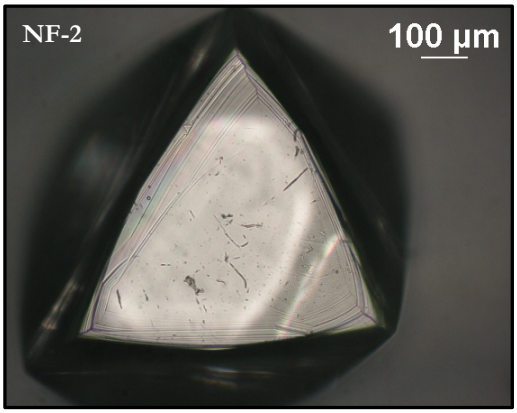

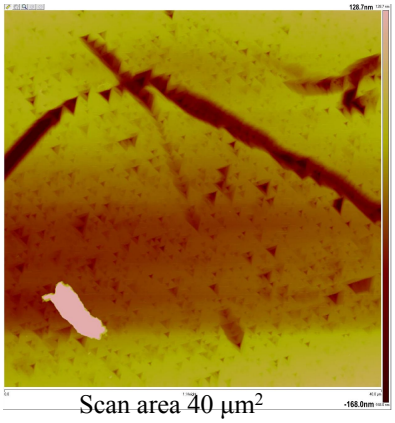

Scan area 40 μm²

In Air for 5.5 hours

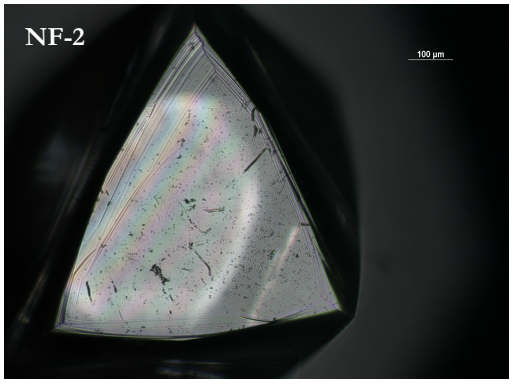

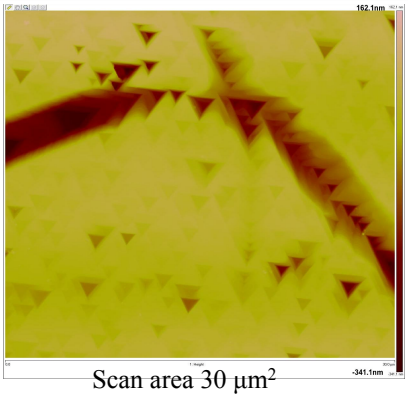

Scan area 30 μm²

Figure 4.1-1 Microphotographs and AFM scans of NF-2 diamond face after each experimental run.

Before the experiment, the studied {111} face of NF-2 diamond crystal had few small flat-bottomed negative trigons with Y-shaped walls. Three negative trigons were measured and were similar in size averaging 4.4 nm depths and 2.1 μm diameters with a minute negative trigons measured to be 1.8 nm deep and 0.5 μm wide.

After the first run at 700 °C for 2.5 hours, NF-2 crystal face {111} produced the following new resorption features:

(1) 100 to 150 μm long grooves of point-bottomed positive trigons with Y-shaped walls,

(2) striation around the crystal face corners,

(3) numerous randomly distributed point-bottomed positive trigons with Y-shaped walls.

11 point-bottomed positive trigons were measured and ranged in depths from 13.5 - 242.1 nm and diameters from 0.3 - 1.8 μm.

After the second run at the same conditions for another 3 hours, the abundance of trigons on the crystal face decreased as the neighbouring trigons grew larger and consumed each other (Figure 4.1-1). Point- and flat-bottomed trigons were produced. Five point-bottomed positive trigons were measured and ranged in depths from 88.3 - 409.1 nm and diameters from 0.61 - 4.8 μm. Five flat-bottomed positive trigons were measured and ranged in depths from 43.5 – 351.5 nm and diameters from 0.9 – 5.1 μm. Two of these flat-bottomed positive trigons evolved from being point-bottomed as shown in Figure 4.1-4. There is a positive correlation between diameter and depth of trigons as resorption progresses, showing diameter to increase with depth (Figure 4.1-2 and Figure 4.1-3). Average vertical dissolution between run 1 and run 2 was estimated to be 108 nm.

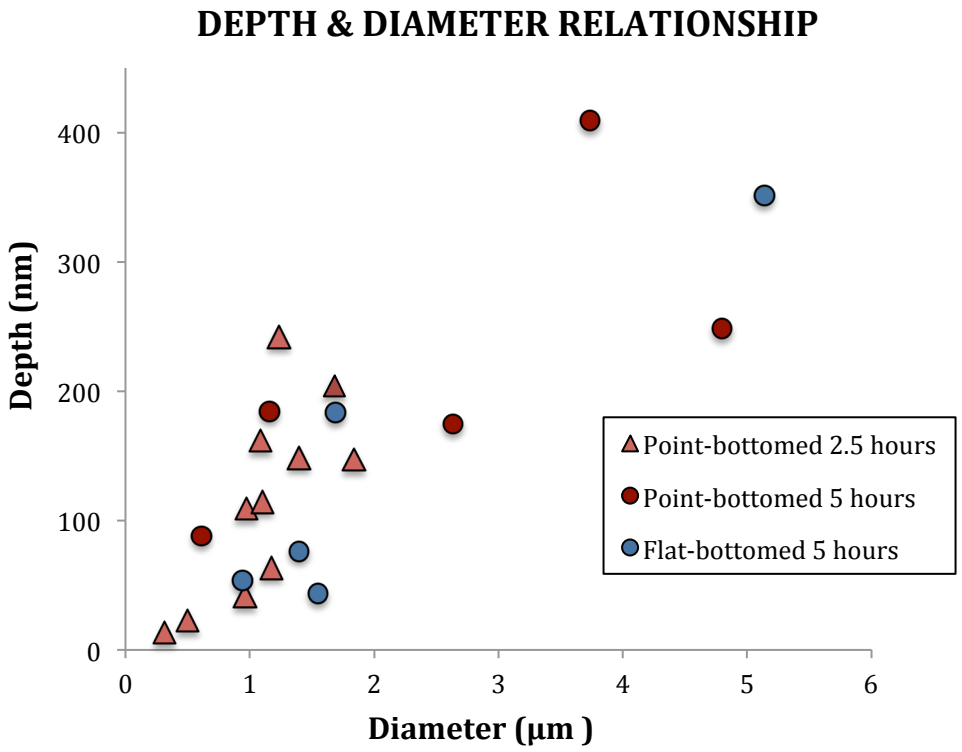

Figure 4.1-2 NF- 2 at 700 °C in air diameter and depth relationship chart (note that the total uncertainty for distance measurements was +/- 2.4%).

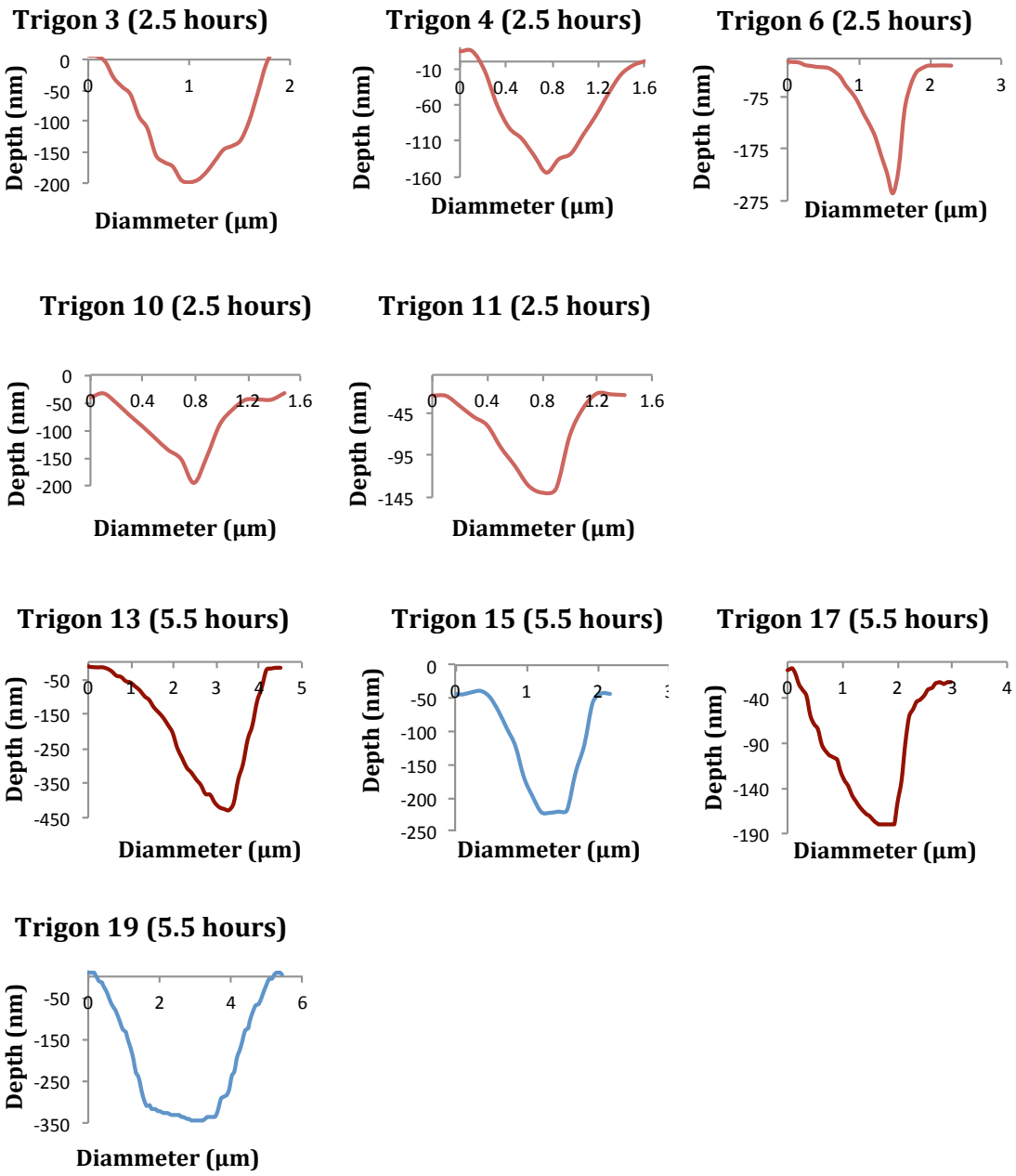

Figure 4.1-3 NF-2 trigon profiles at 700 °C in air.

Evolution of four point-bottomed positive trigons (3, 4, 10 and 11) after 2.5 hours and 5 hours at 700 °C in air can be see via depth and diameter profiles (Figure 4.1-4 and Figure 4.1-5). Trigon 3 and 11 show evolution in bottom shape from point to flat and it is possible that this change is as a result of on going resorption at these conditions.

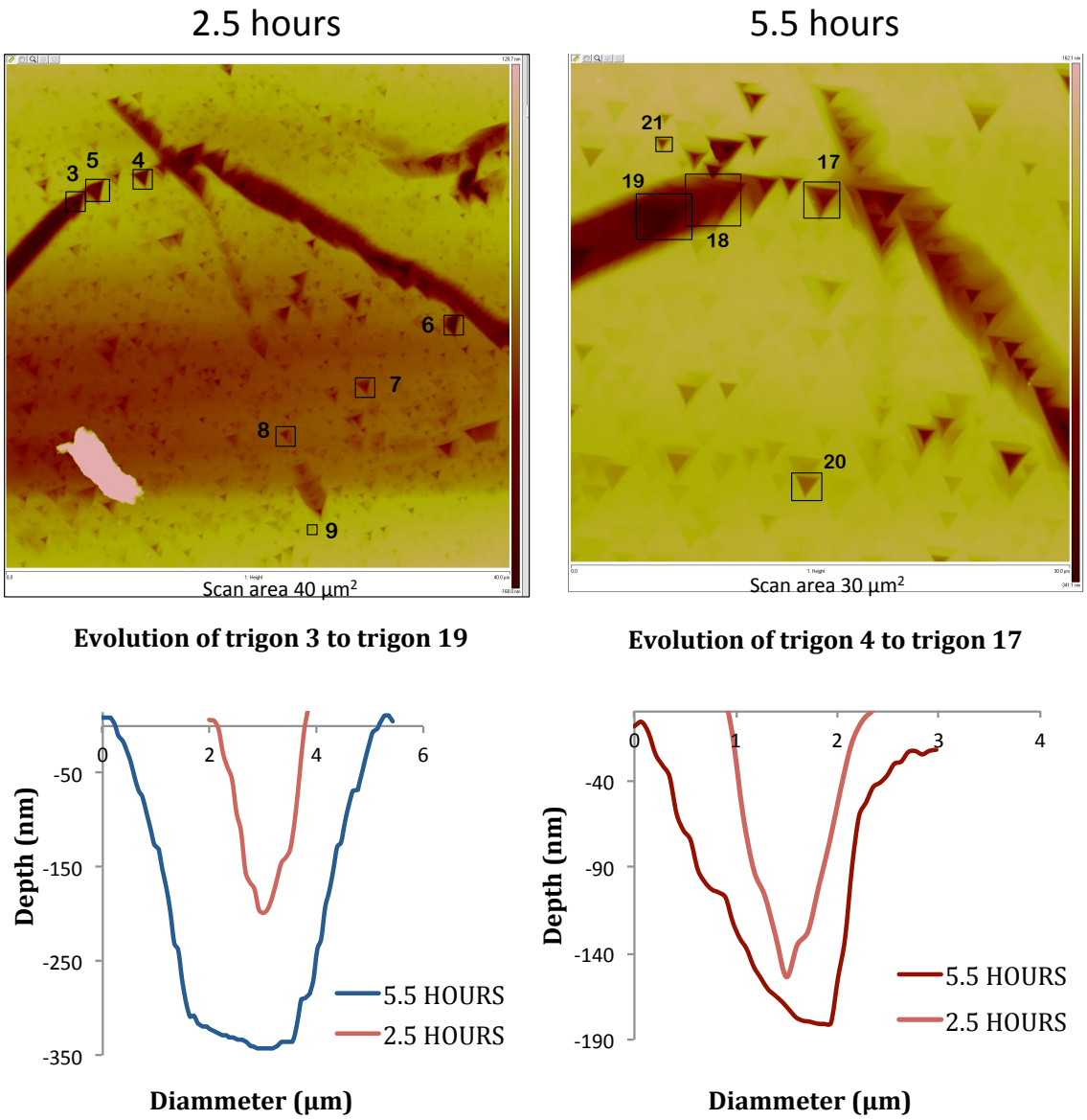

Figure 4.1-4 Evolution profiles of trigon 3 and 4 to trigon 19 and trigon 17 respectively with their corresponding AFM scans.

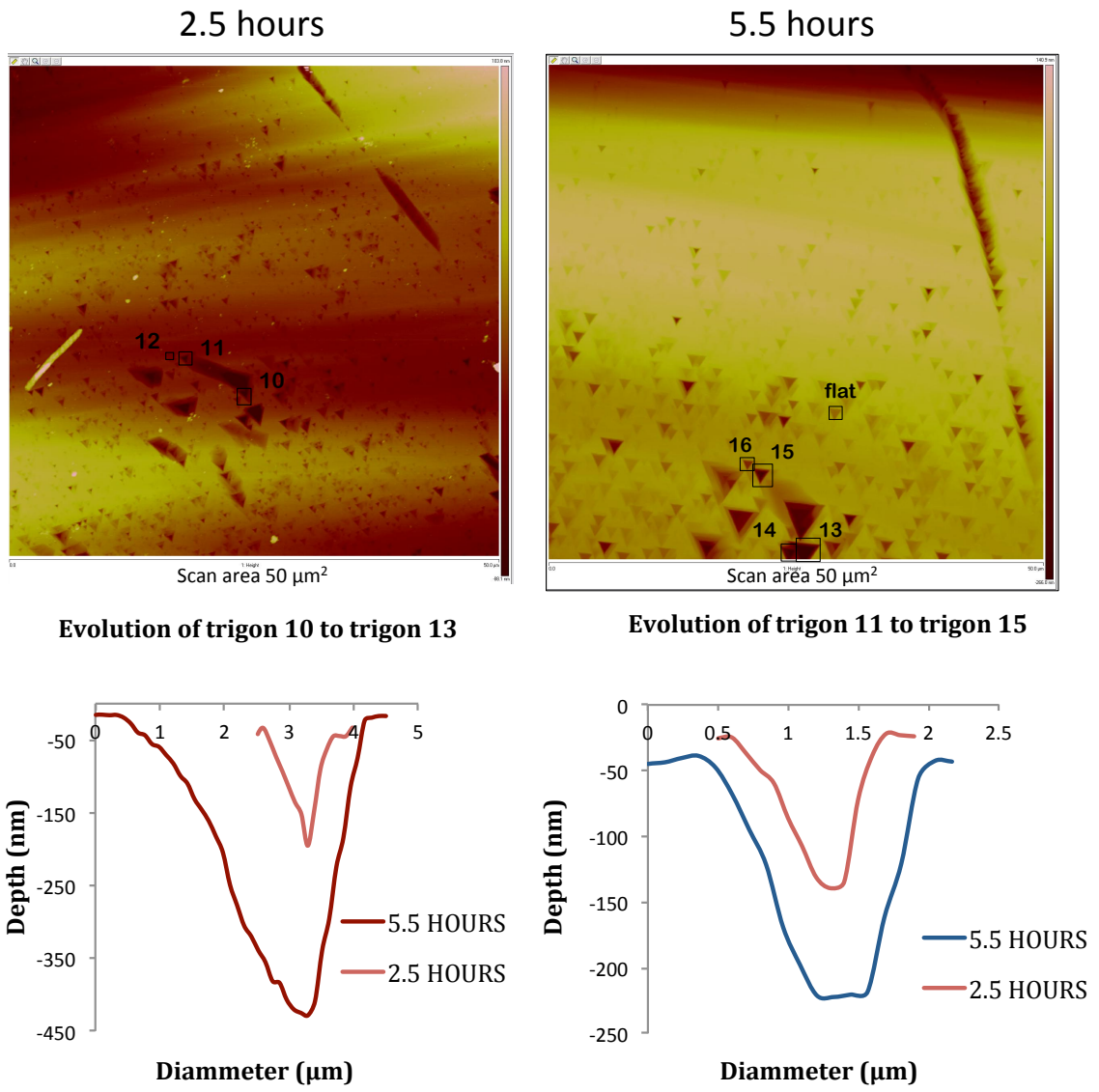

Figure 4.1-5 Evolution profiles of trigon 10 and 11 to trigon 13 and trigon 15 respectively with their corresponding AFM scans.

4.2 Experiments at 800 °C in Air

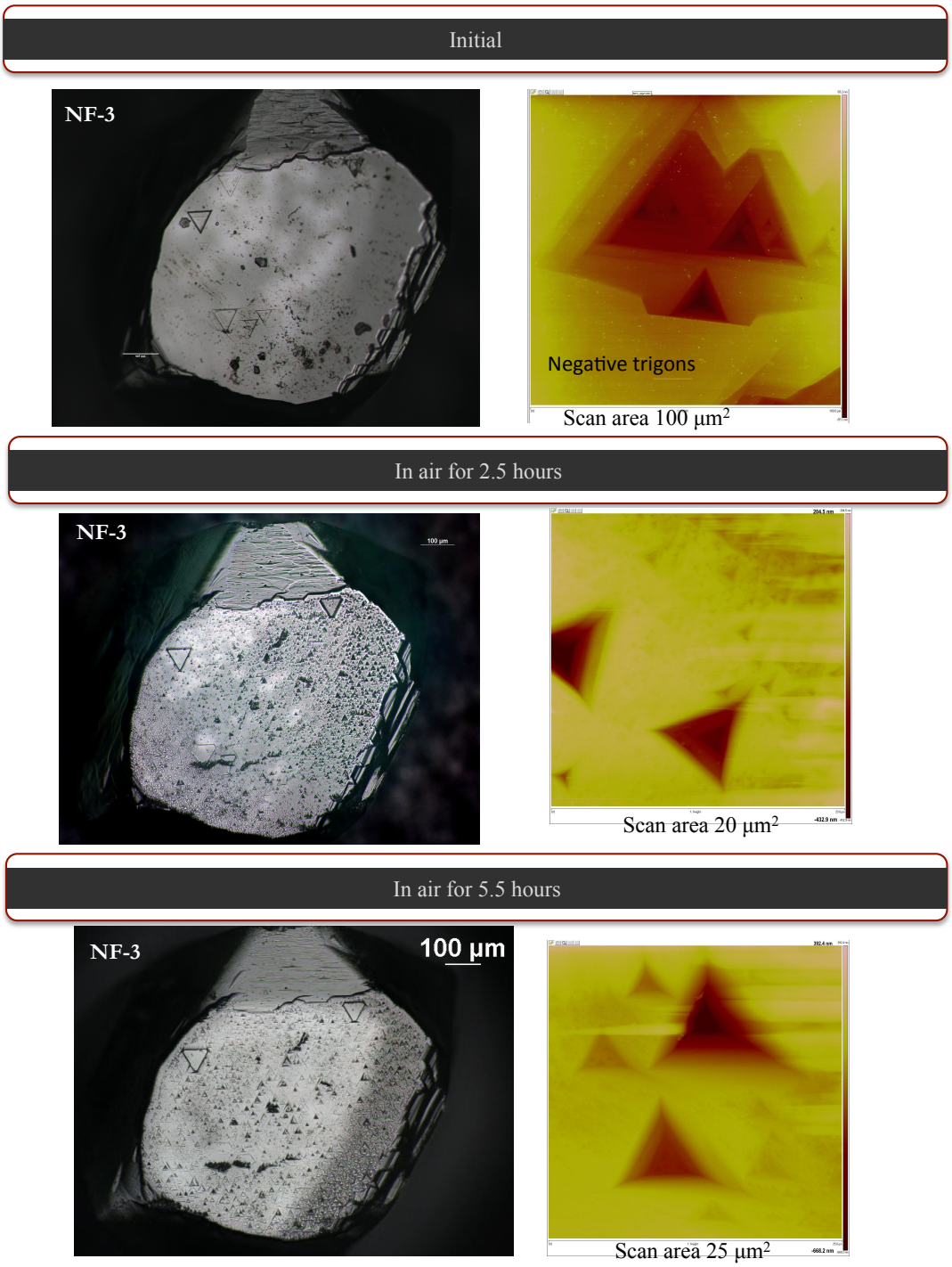

Figure 4.2-1 Microphotographs and AFM scans of NF-3 diamond face after each experimental run.

Before the experiment, the studied {111} face of NF-3 diamond crystal had few point-bottomed negative trigons with Y-shaped walls. Two point-bottomed negative trigons were measured and ranged in size with one 93.4 nm deep and 18 μm wide and the other 15.4 nm deep and 2.5 μm wide (Figure 4.2-1).

After the first run at 800 °C for 2.5 hours, diamond produced resorption features including:

(1) > 100 μm long grooves of positive trigons,

(2) striation around the face corners,

(3) point-bottomed positive trigons with Y-shaped walls with a wide size range,

(4) a few flat-bottomed positive trigons with Y-shaped walls.

A higher abundance of positive trigons is observed around the crystal face corners compared to the rest of the face. Apexes of pre-existing negative trigons were truncated and some have been etched over with positive trigon grooves (Figure 4.2-1). Five point-bottomed positive trigons were measured and ranged in depth from 18.9 - 724.6 nm and diameters from 0.4 – 6.8 μm. Two flat-bottomed positive trigons were measured and have similar diameters of 3.9 μm and depths of 68.5 and 166.1 nm.

After the second run for another 3 hours at the same conditions, the overall trigon abundance on the crystal face decreased, although the abundance of the trigons around the crystal corners increased (Figure 4.2-1). Trigon abundance decrease can be explained by neighbouring trigon consuming each other as they grow in size. Limited AFM scans were taken due to high density of trigons on the crystal face. Three point-bottomed positive trigons were measured and ranged in depths from 343.1 – 992 nm and diameters from 6.4 – 12.3 μm. One flat-bottomed positive trigon was measured to be 301.8 nm deep and 10.3 μm wide. Two out of four pre-existing negative trigons completely disappeared. There is a positive correlation between diameter and depth of trigons as resorption progresses showing diameter to increase with depth (Figure 4.2-2 and Figure 4.2-3). Average vertical dissolution between run 1 and run 2 was estimated to be 314.6 nm.

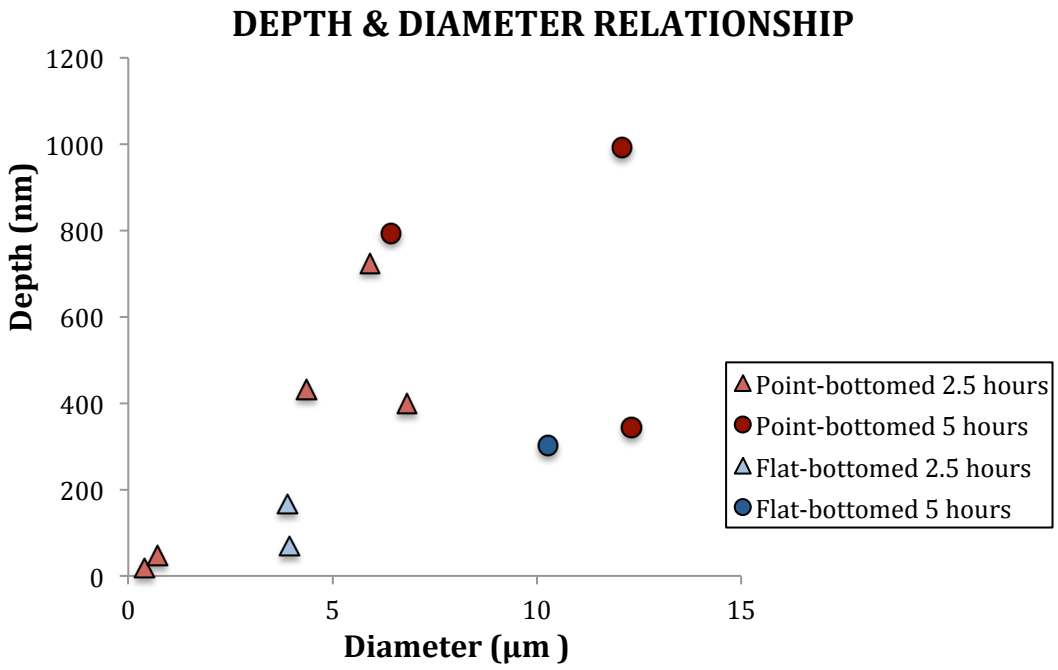

Figure 4.2-2. NF- 3 at 800 °C in air diameter and depth relationship chart (note that the total uncertainty for distance measurements was +/- 2.4%).

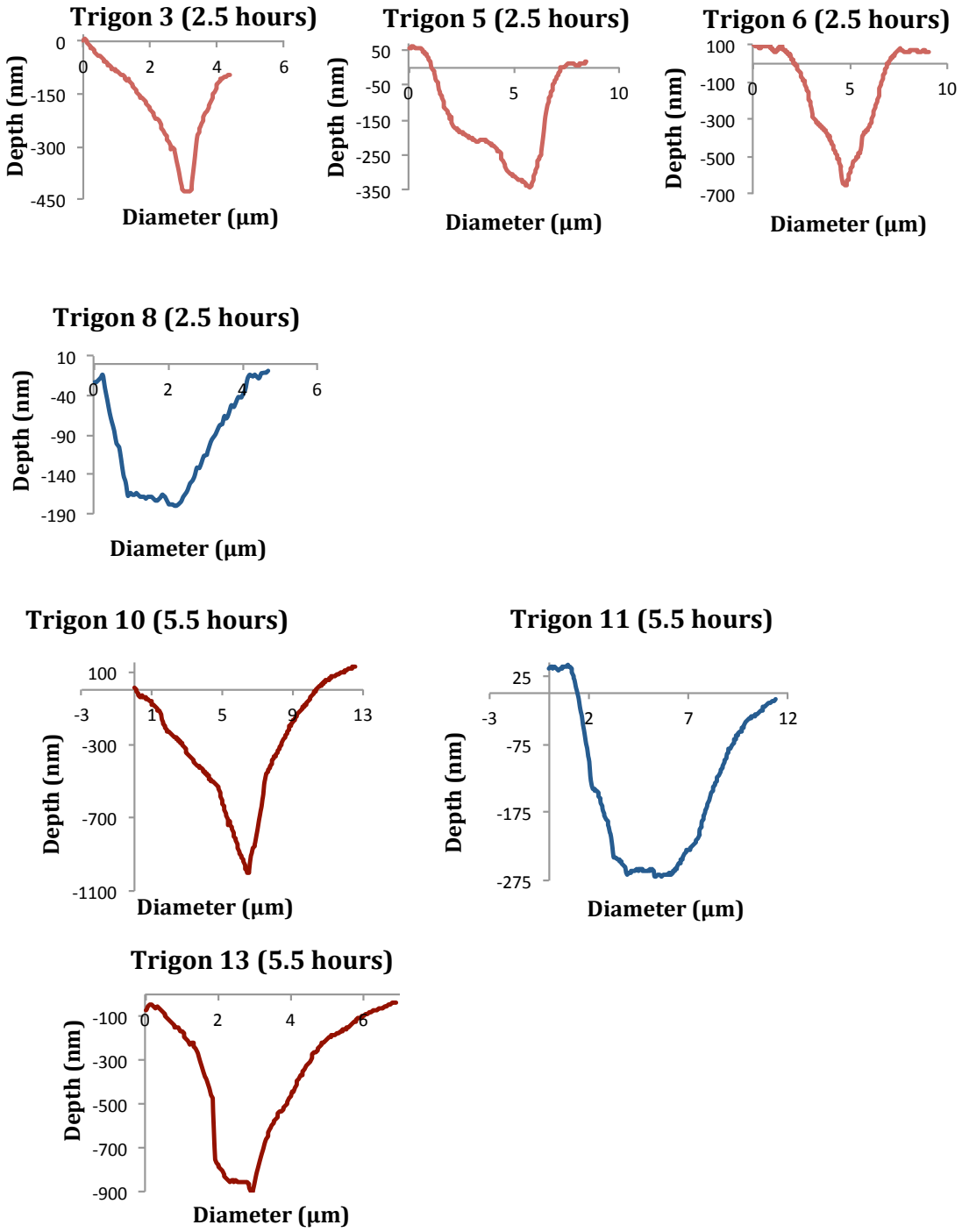

Figure 4.2-3 NF-3 trigon profiles at 800 °C in air.

NF-3 positive trigons morphology showed no evolution of bottom shape as resorption progressed (Figure 4.2-4 and Figure 4.2-5) and trigon abundance decreased on the crystal face as neighboring trigons grew larger and consumed each other.

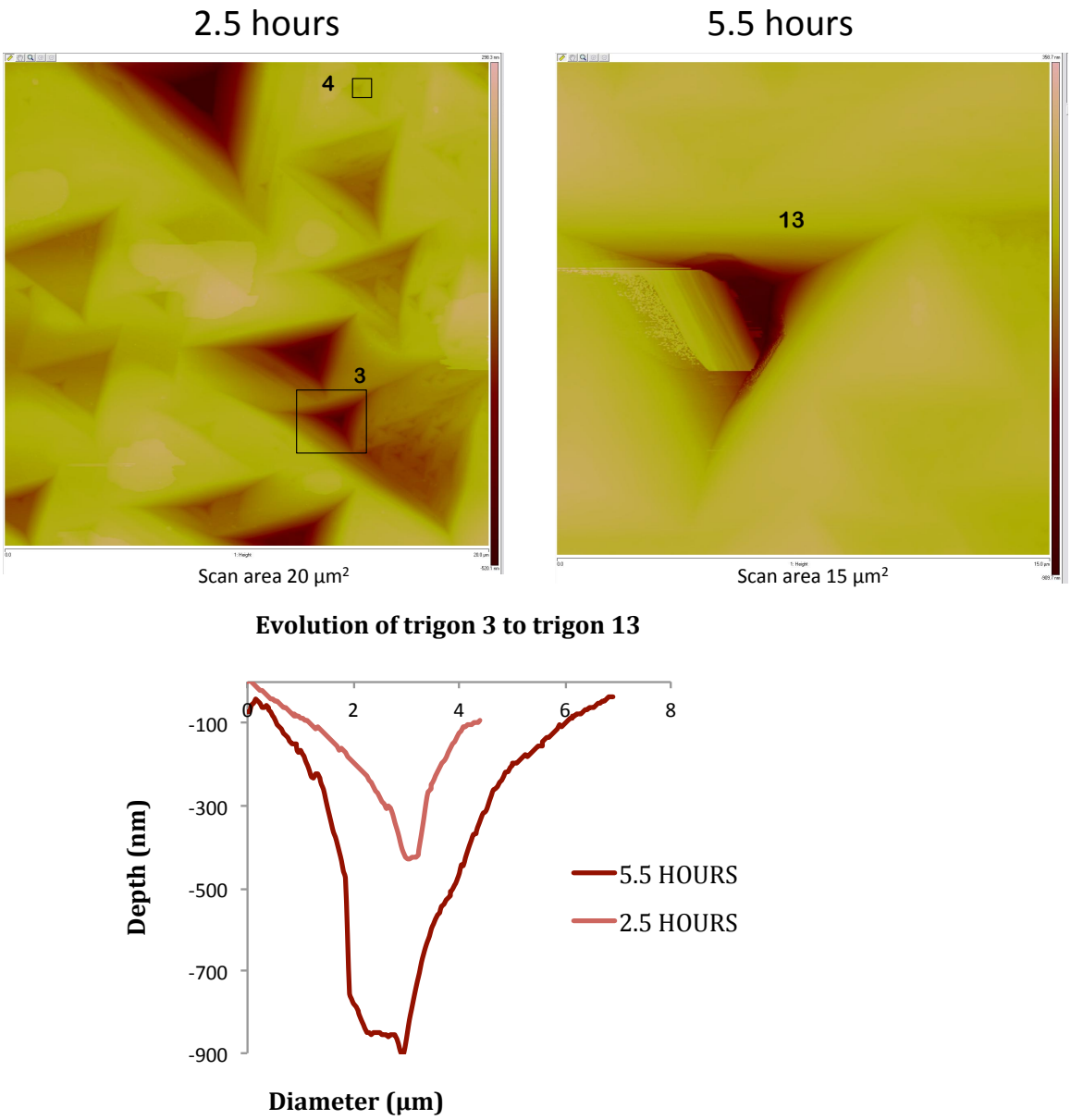

Figure 4.2-4 Evolution profile of trigons 3 to trigon 13 with corresponding AFM scans.

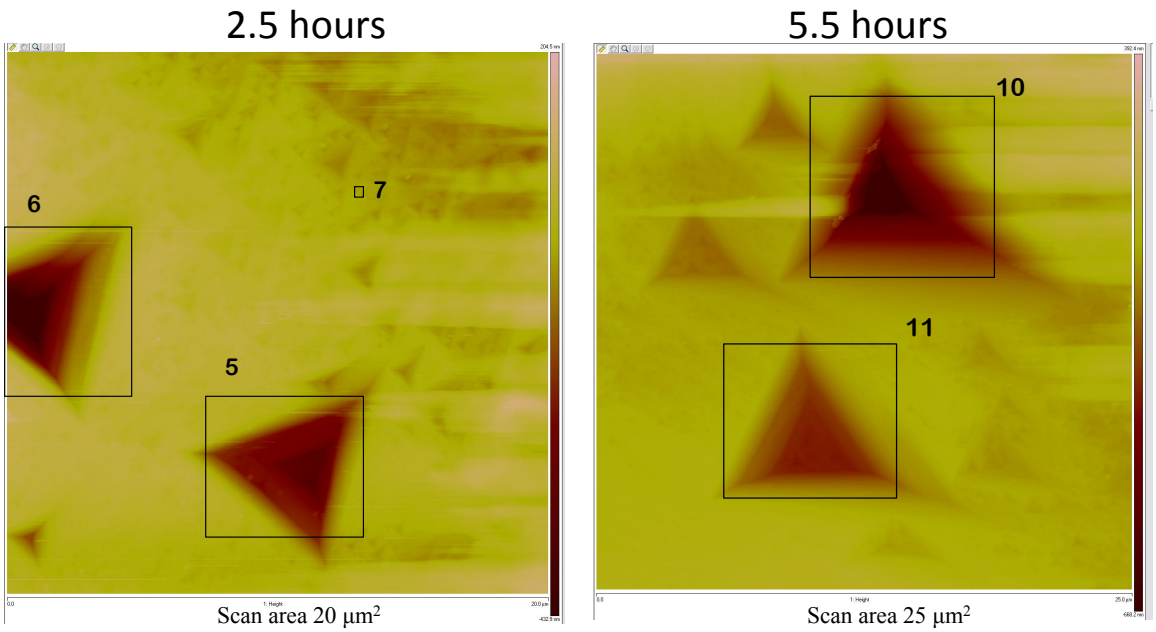

Evolution of trigon 6 to trigon 10

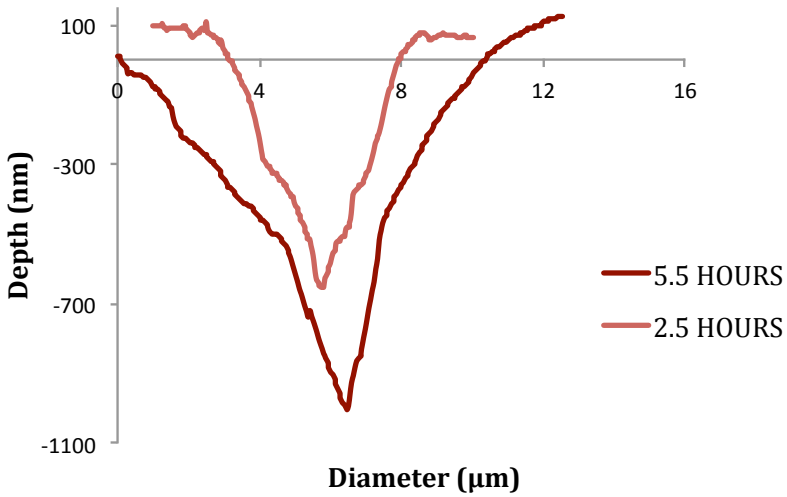

Figure 4.2-5 Evolution profile of trigon 6 to trigon 10 with corresponding AFM scans.

In summary, diamond resorption in air at 700 °C and 800 °C both produced positive trigons and grooves of positive trigons. After 2.5 hours (run 1) at 700 °C, the largest positive trigon depths and diameters were 242 nm and 1.8 μm, which are much smaller at 800 °C with depths and diameters of 724.6 nm 5.9 μm. Positive trigons produced at 700 °C were all point-bottomed and less abundant than positive trigons at 800 °C, which were mostly point-bottomed with a few flat (Figure 4.2-6).

After 5.5 hours (run 2) the abundance of trigons was higher at 800 °C compared to 700 °C, and the largest positive trigon depths and diameters at 700 °C were 409 nm and 5.1 μm. At 800 °C the largest positive trigon depths and diameters were 992 nm and 12.3 μm (Figure 4.2-6). A few point-bottomed positive trigons at 700 °C evolved to flat-bottomed as they grew in size as resorption progressed, but at 800 °C both point- and flat-bottomed positive trigons grew in size and retained their shape. Vertical dissolution was calculated to be greater at 800 °C than at 700 °C by 196.3 nm. Hence, higher temperature (800 °C) etched larger positive trigons with predominantly point-bottomed trigons and a few flat-bottomed trigons. Table 4.1 summarizes the positive trigons dimensions from both experiments at 700 °C (NF-2) and 800 °C (NF-3) in air.

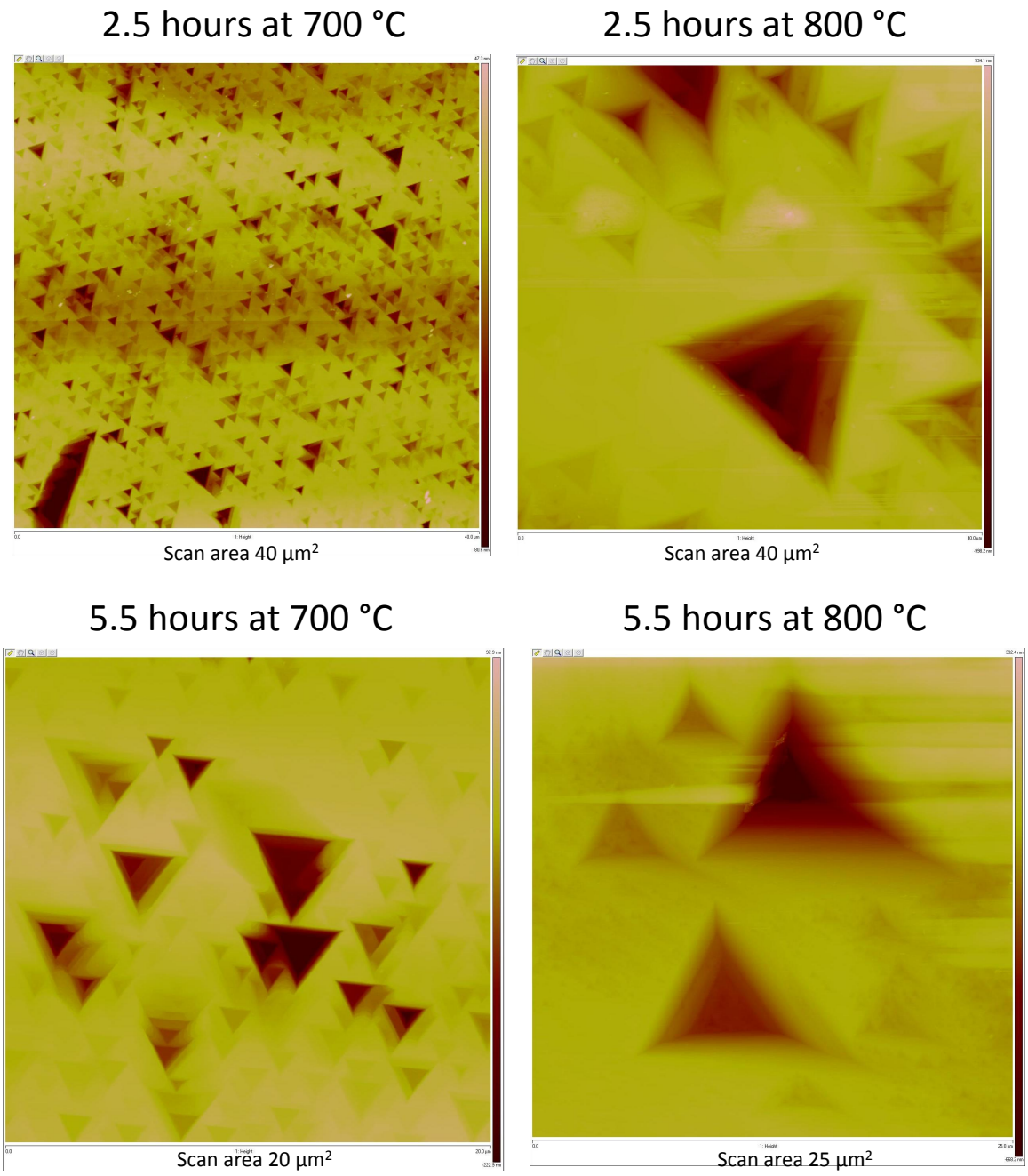

Figure 4.2-6 AFM scan of diamond crystal face after 2.5 hours (run 1) and 5 hours (run 2) at 700 °C and 800 °C in air (similar scan size).

Table 4.1 Dimensions of positive trigons at 700 °C (NF-2) and 800 °C (NF-3).

Diamond Sample	Average Depth Run 1 (nm)	Average Depth Run 2 (nm)	Average Diameter Run 1 (μm)	Average Diameter Run 2 (μm)	Dominant Wall & Bottom Shape Run 1	Dominant Wall & Bottom Shape Run 2
NF-2						
Small (8)	35.24	65.40	0.69	0.78	Y-shaped, point-bottomed	Y-shaped, point-bottomed
Large (12)	161.09	258.63	1.36	2.76	Y-shaped, point-bottomed	Y-shaped, point-bottomed
NF-3						
Small (5)	44.59	322.44	1.22	6.44	Y-shaped, point-bottomed	Y-shaped, point-bottomed
Large (6)	430.75	893.10	4.99	11.56	Y-shaped, point-bottomed	Y-shaped, point-bottomed

4.3 Experiments at 700 °C in Pure CO_2

This experiment ran for 3.5 hours and did not produce any surface resorption features (Figure 4.3-1) therefore we can conclude that diamond resorption does not occur in Na_2CO_3-NaCl melt at 700 °C at atmospheric pressure (0.1 MPa) in atmosphere of CO_2 (log fO_2 = -2.85).

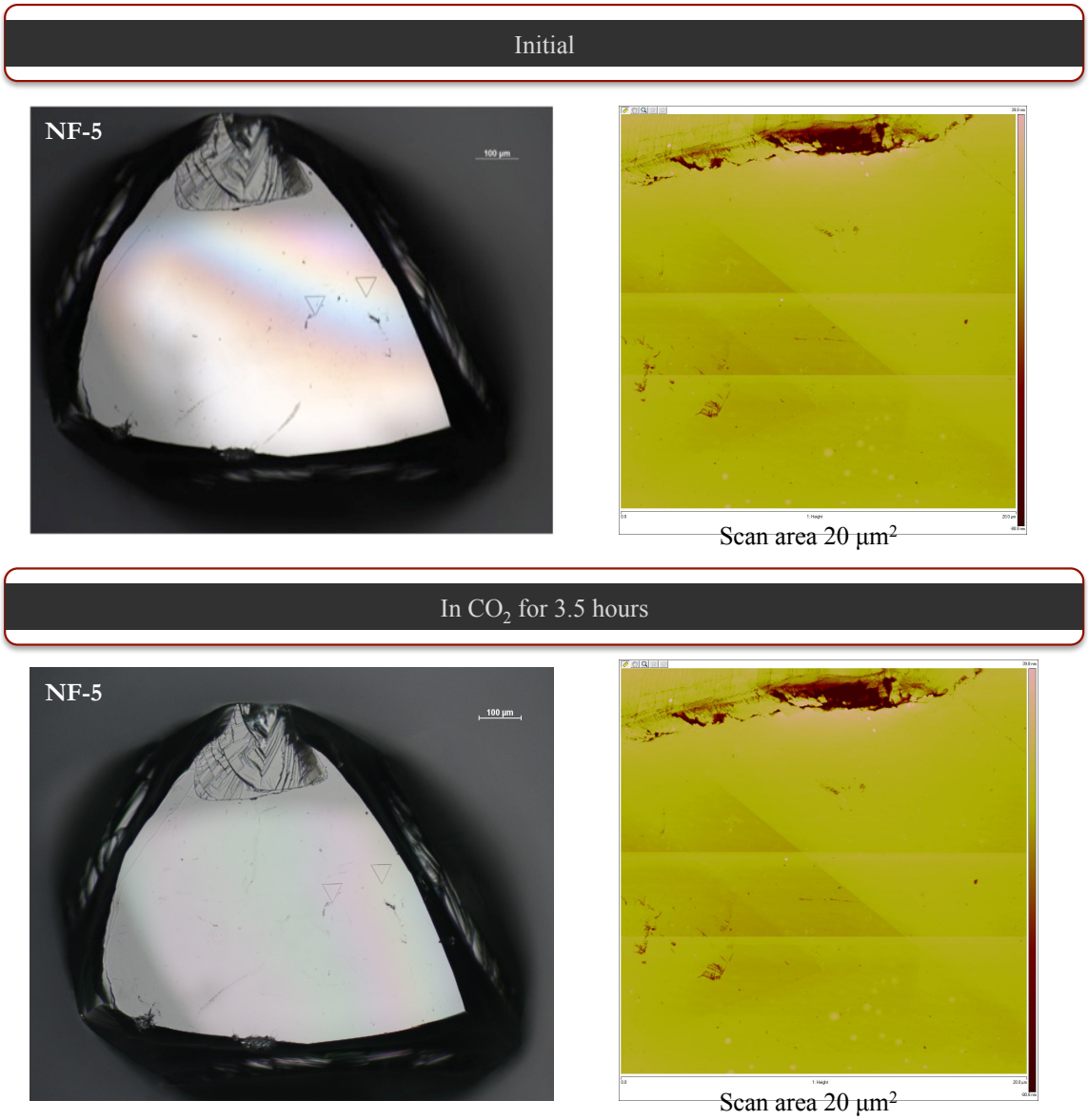

Figure 4.3-1 Microphotographs and AFM scan of NF-5 diamond face after 3.5 hours experimental run.

4.4 Experiments at 800 °C in pure CO_2

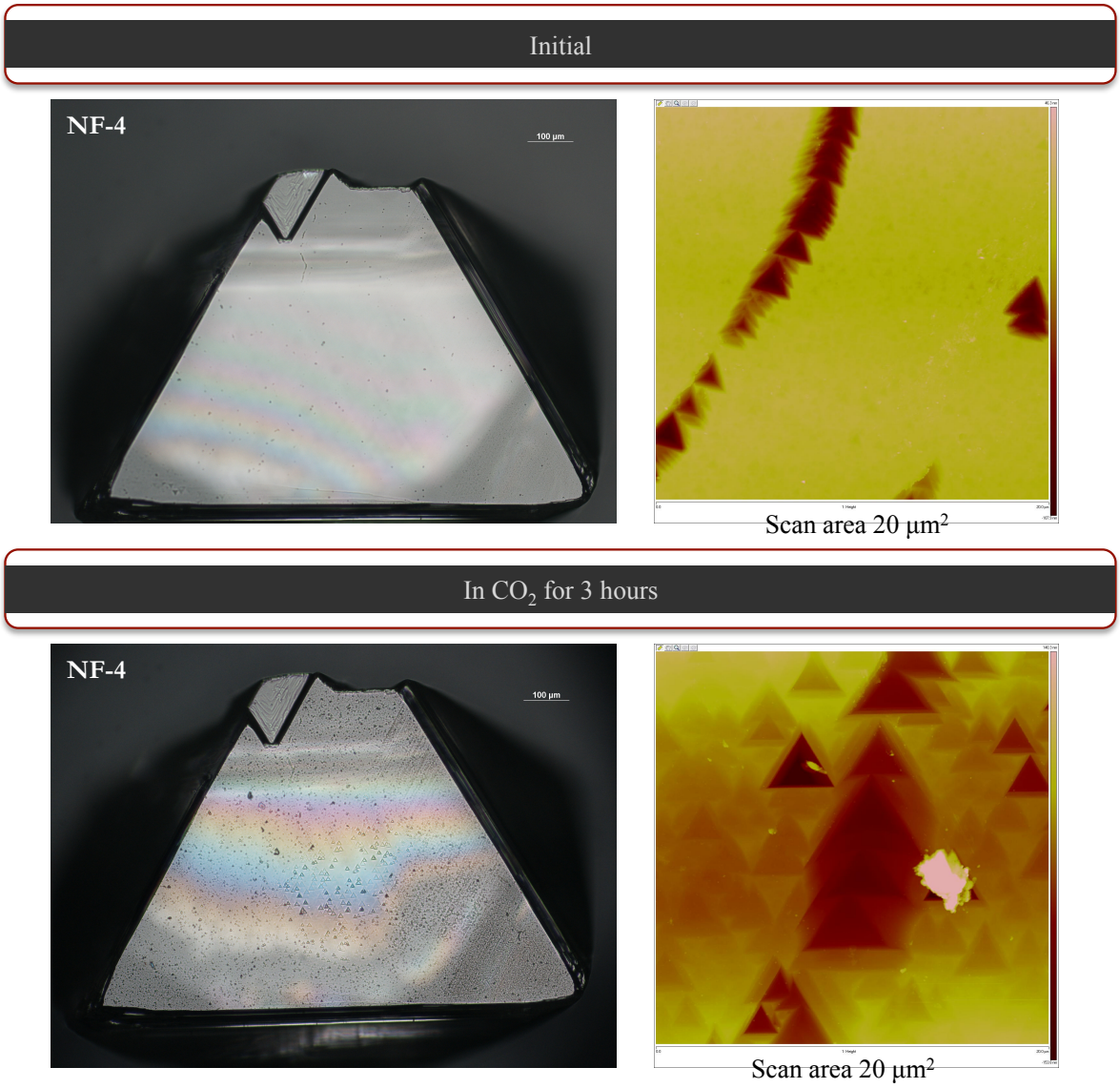

Figure 4.4-1 Microphotographs and AFM scans of NF-4 diamond face after 3 hour experimental run.

Before the experiment, the studied {111} face of NF-4 diamond crystal had a groove of small point-bottomed positive trigons with Y-shaped walls (Figure 4.4-1). The positive trigon measured in the groove was 93.9 nm deep and 2.2 µm wide. A few flat-bottomed negative trigons with Y-shaped walls were present (Figure 4.4-1). One flat-bottomed negative trigon was measured to be 80 nm deep and 12.2 µm wide. This negative trigon

had a small point-bottomed positive trigons etched in it's centre which was measured to be 32.8 nm deep and 1.3 μm wide.

After the first run in CO_2 (log fO_2 = -2.79) at 800 °C for 3 hours, NF-4 crystal face {111} produced new resorption features:

(1) < 30 μm long grooves of flat-bottomed positive trigons with Y-shaped walls,

(2) few flat-bottomed positive trigons with Y-shaped walls in the middle,

(3) numerous small point-bottomed positive trigons etched in the centre and around pre-existing negative trigons,

Abundance of positive trigons in the middle of the crystal face was less than around the corners (Figure 4.4-1), and were all flat-bottomed positive trigons ranging in size with depths from 80.9 – 419.6 nm and diameters from 5.8 – 13.2 μm. Four point-bottomed positive trigons were measured around the crystal face corners and ranged in size with depths from 52.7- 185.1 nm and diameters from 0.9 – 4 μm. One flat- bottomed positive trigon in one of the grooves was measured to be 5.8 μm wide and 99.5 nm deep. Pre-existing negative trigon remained the same size but had point-bottomed positive trigons etched inside them. Flat-bottomed trigons measured had diameters > 5 μm and point-bottomed had diameters < 5 μm (Figure 4.4-2 and Figure 4.4-3). Table 4.4 list dimensions of measured positive trigons produced at 800 °C in CO_2.

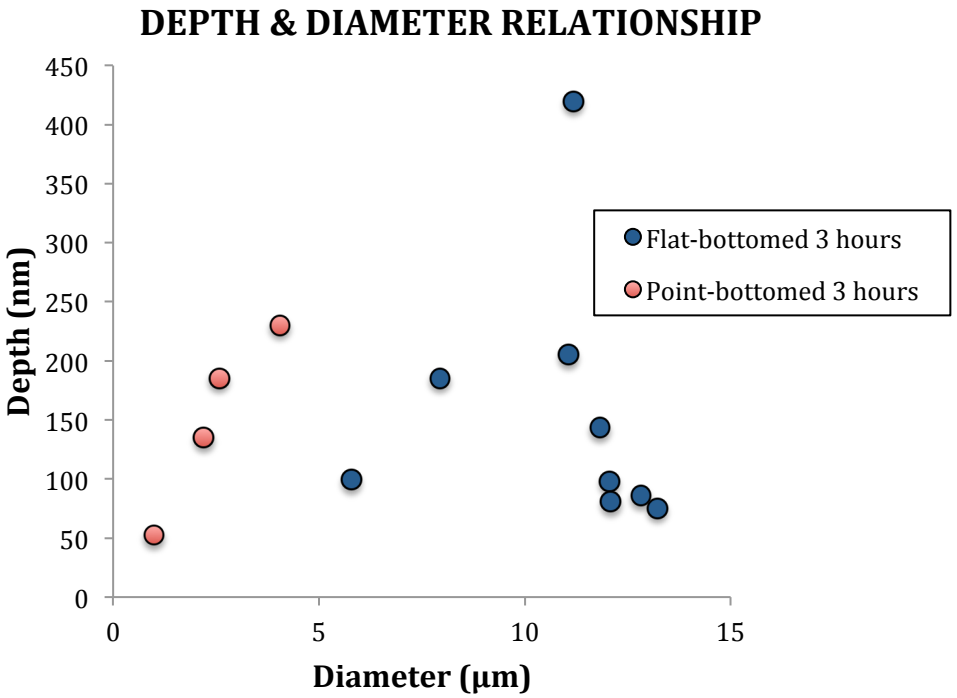

Figure 4.4-2. NF- 4 at 800 °C in CO_2 diameter and depth relationship chart (note that the total uncertainty for distance measurements was +/- 2.4%).

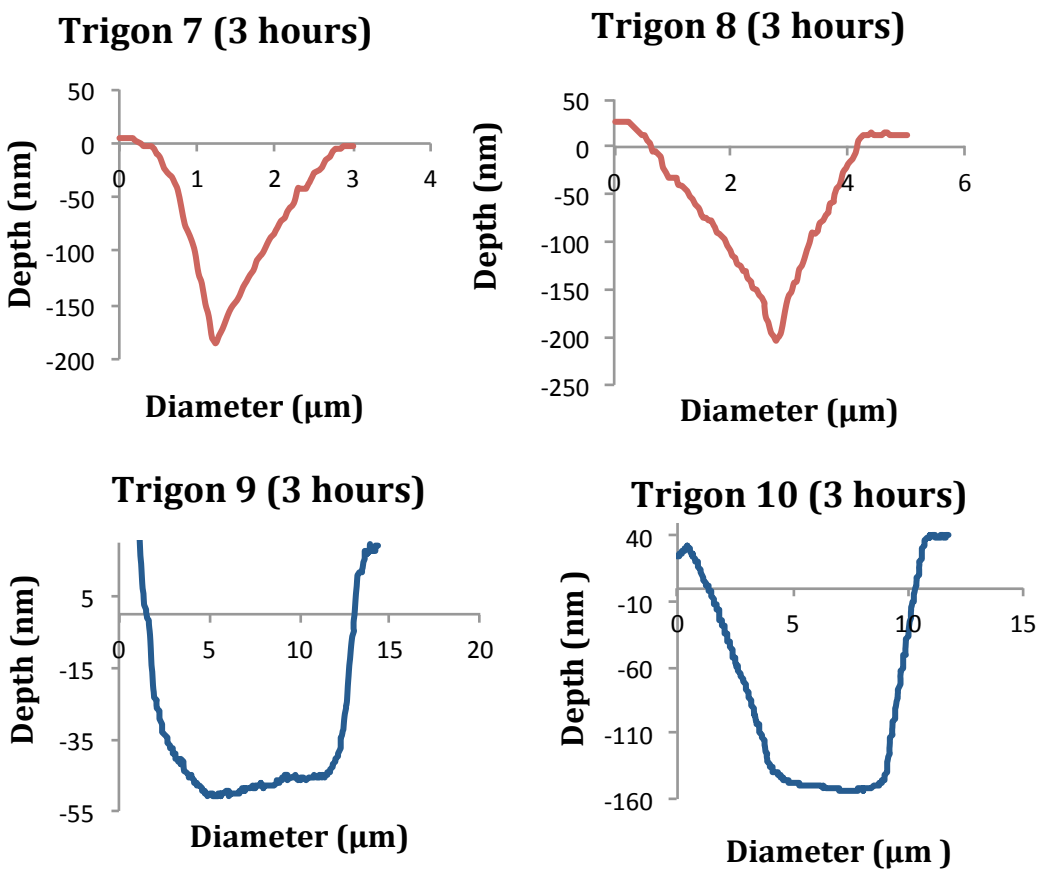

Figure 4.4-3 NF-4 trigon profiles at 800 °C in CO_2.

Table 4.4 Dimensions of positive trigons produced at 800 °C in CO_2.

Diamond Sample	Average Depth Run 1 (nm)	Average Diameter Run 1 (µm)	Dominant Wall & Bottom Shape Run 1
NF-4			
Small (7)	140.46	3.12	Y-shaped, point-bottomed
Large (6)	161.78	11.53	Y-shaped, flat-bottomed

In summary, diamond dissolution at 800 °C in air (log fO_2 = -0.68) and in CO_2 (log fO_2 = -2.79) both produced mostly point-bottomed trigons and a few flat-bottomed. After 2.5 hours in air point-bottomed positive trigons that were measured recorded a maximum depth of 724 nm and diameter of 5.9 µm, which are much larger than the point-bottomed positive trigons in CO_2 after 3 hours, which recorded a maximum depth of 230.1 nm and diameter 4 µm. The flat-bottomed positive trigons in air that were measured recording a maximum depth of 166.1 nm and diameter of 3.9 µm, which were smaller than the largest of flat-bottomed positive trigons in CO_2 with depth of 419.6 nm and diameter of 13.2 µm (Figure 4.4-4).

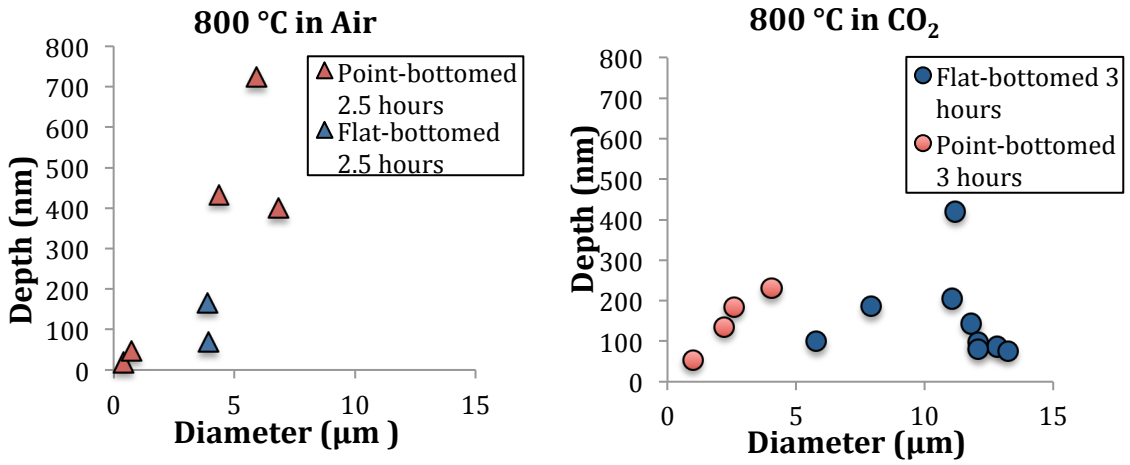

Figure 4.4-4. Depth and diameter charts of positive trigons at 800 °C in air for 2.5 hours and in CO_2 for 3 hours (note that the total uncertainty for distance measurements was +/- 2.4%).

5. DISCUSSION AND CONCLUSIONS

5.1 Factors Controlling Trigon Morphology

5.1.1 Halogen Presence

Keltie et al. (2016) examined how the presence of halogens in carbonate kimberlite melt affects the morphology of positive trigons. Experiments used melt compositions of Na_2CO_3, Na_2CO_3-NaCl, and Na_2CO_3-NaF at 950ºC at atmospheric pressure (0.1 MPa) (Keltie et al., 2016). Keltie (2106) observed that Na_2CO_3-NaCl melt developed more kink sites for carbon atoms to be removed compared to the other two compositions. Keltie et al. (2016) suggested that the strong electronegativity of Cl weakened the C-C bond between the carbon atoms on the surface of the diamond allowing relatively easier carbon atoms removal. Previous study by Rudenko et al. (1967) proposed that the presence of Cl in the carbonate melt alters the HCO complexes to form Cl-C-O complexes, and the strong electronegativity of Cl disrupts the carbon atom bonds in the diamond crystal lattice making removal of bonded carbon easier. Therefore, during diamond resorption near the surface in Cl-carbonate kimberlite melts, positive trigons can be easily etched by the easy removal of three-bonded carbon atoms from the diamond crystal lattice.

5.1.2 Temperature

Comparing this study's experiments at 700 °C and 800 °C in air after 2.5 hours to Keltie et al. (2016) at 950 °C in air after 2 hours confirms a temperature effect on positive trigon morphology. At 950 °C after 2 hours mostly flat-bottomed positive trigons were produced and measured depths ranged from 52.8 – 591.6 nm and diameters from 2.5 – 24.5 μm, and a few point-bottomed positive trigons were produced with higher depths up to 1133 nm and diameters up to 26.9 μm (Figure 5.1.2-1). Increase in temperature is seen to increases positive trigons size and initial the trigon abundance on the crystal face. Two trends of trigon evolution are observed as temperature increases from 700 °C to 800 °C to 950 °C for 2 – 2.5 hours (Figure 5.1.2-1):

(1) point-bottomed positive trigons grow significantly in depth and diameter showing a positive correlation between the two,

(2) flat-bottomed positive trigons grow in depth and diameter but not to significantly (most diameter below 10 μm and depths below 400 nm).

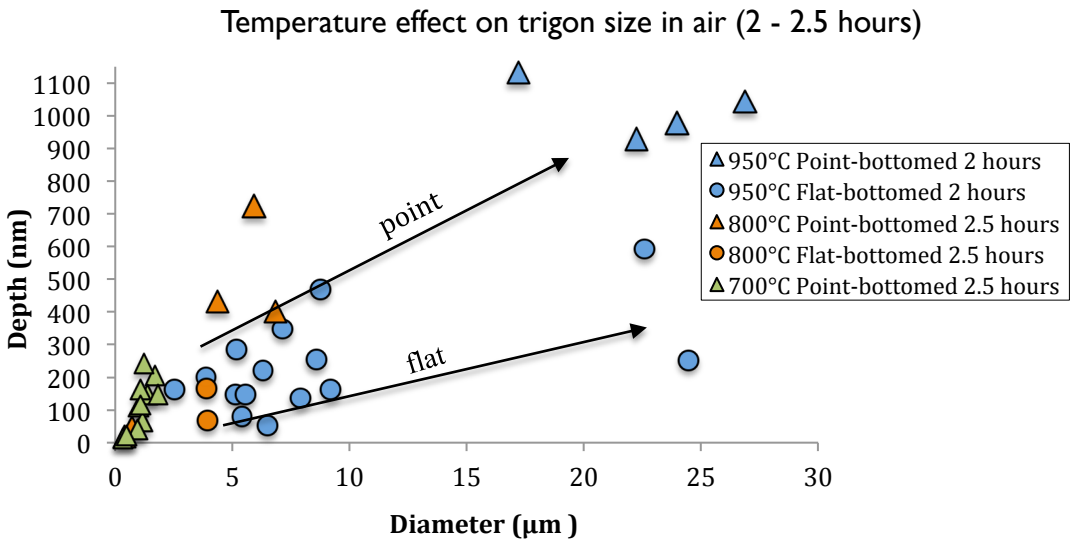

Figure 5.1.2-1. 950 °C in air for 2 hours and 700 °C, 800 °C for 2.5 hours temperature effect on positive trigons size (note that the total uncertainty for distance measurements was +/- 2.4%).

The relative effects of temperature and resorption duration are important factors that should be considered when examining trigon morphology. Both temperature and resorption duration increase the size of trigons. Although it has been established that resorption at higher temperatures etch larger trigons than at lower temperatures, we still need to constrain the extent to which resorption time affects the size and morphology of positive trigon after it has been etched.

5.1.3 Oxygen fugacity

Comparing different positive trigon morphology produced at 800 °C in air ($\log fO_2$ = -0.68) and in pure CO_2 ($\log fO_2$ = -2.79) confirms that increase in oxygen fugacity from very oxidizing conditions (air) to slightly less oxidizing conditions (CO_2) produces two different trigon evolution trends for point-bottomed and flat-bottomed positive trigons (Figure 5.1-3):

(1) point-bottomed positive trigons grow in depth and diameter showing a positive correlation,

(2) flat-bottomed positive trigons decrease in diameters and hardly change in depth.

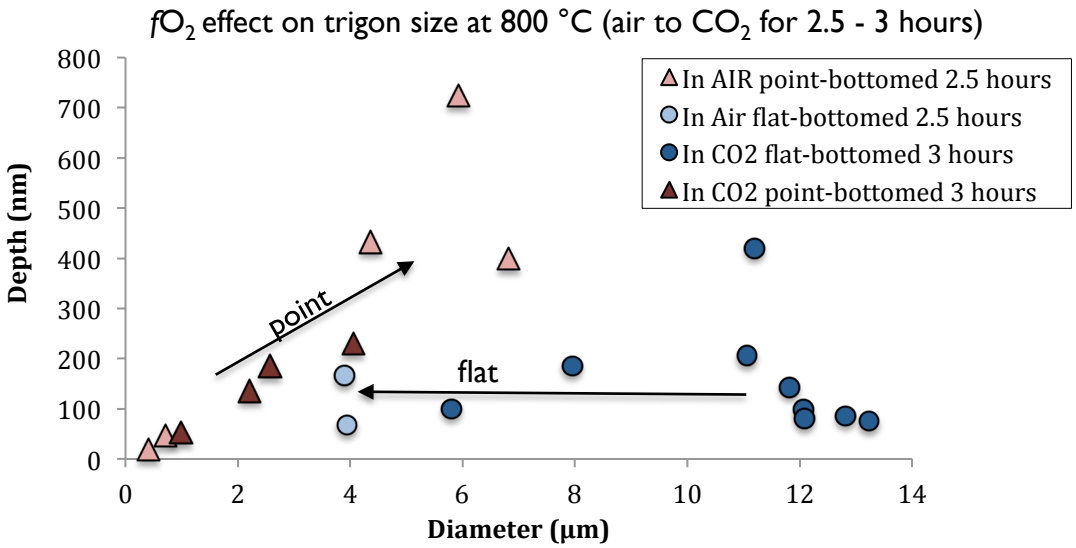

Figure 5.1.3-1. 800 °C in air for 2.5 and CO_2 for 3 hours oxygen fugacity effect on positive trigons size (note that the total uncertainty for distance measurements was +/- 2.4%).

Positive trigon abundance on the crystal face increases towards more oxidizing conditions (air). This slight increase in oxygen fugacity has opposite effects on the mechanism of diamond resorption on the diamond crystal {111} face; vertical resorption (perpendicular to {111} face) is dominant for point-bottomed trigons, and horizontal resorption (parallel to {111} face) is dominant for flat-bottomed positive trigons (Figure 5.1.3-2).

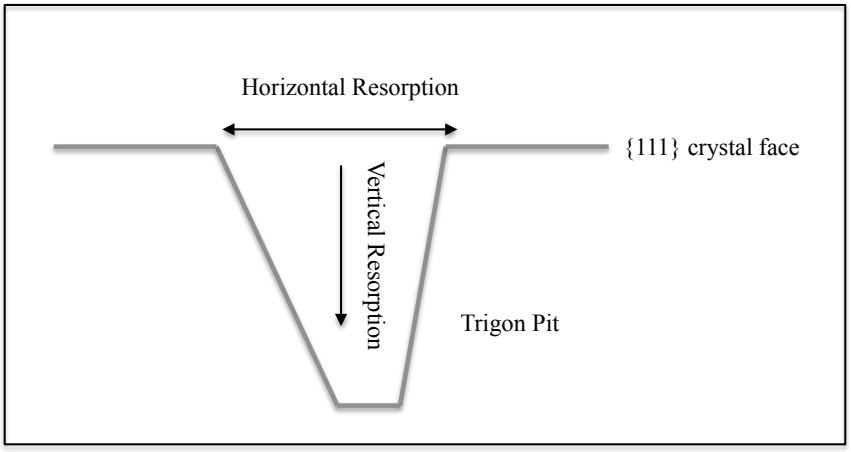

Figure 5.1.3-2 Horizontal vs. Vertical Resorption on {111} crystal face.

5.2 Relative effects of internal and external factors on trigon morphology

Trigon morphology can be controlled by internal factors such as the type of defects present in the diamond crystal lattice or by external factors such as kimberlite melt composition, temperature, pressure and oxygen fugacity. The relative effects of each the factors can cause either only one or two types of trigons (point/flat) to develop on diamond crystal face during resorption. If only one type of trigon morphology develops on diamond crystal face then external factors have the main control on trigon morphology however, if two or more different types of trigon morphologies develop under unchanged resorption conditions then the external factors conditions as well as the type of defects present have the main control. None of the experiments produced one type of positive trigon morphology; hence the external conditions and defects are both affected the trigon morphology produced.

Previous experimental studies such as Khokhryakov et al. (2006) have proposed a relationship between the type of defects on the crystal face and the bottom shape of etched trigon pits. Using a number of methods including repeated etching, etching of thin cleavage plates, Khokhryakov et al. (2006) proposed that point-bottomed trigons are formed at dislocations, initial positive trigons are formed at screw and partial dislocations and flat-bottomed trigons are formed at surface defects such as impurities and microcracks. Khokhryakov et al. (2006) concluded that initial trigons etched are small and point-bottomed, and deeper point-bottomed and flat-bottomed trigons are secondary. Experiments in this study confirm initial trigons to be point-bottomed and as resorption progresses flat-bottomed and deeper point-bottomed trigons develop.

5.3 Application to Snap Lake Kimberlite

5.3.1 Overview of Positive trigons of Snap Lake Kimberlite Dike

Any diamond population has a high proportion of diamonds with negative trigons. Positive trigons, on the contrary, are very rare. Snap Lake kimberlite dike in Northwestern Territories, Canada have abundant positive trigons on all diamonds whereas Ekati kimberlite pipe diamonds do not show the same abundance of positive trigons. Li (unpublished data, February 2017) proposes that this unusual occurrence of abundant positive trigons on Snap Lake diamonds could be caused by a later resorption

event of which the prevalent conditions are unknown. Petrographic and mineralogical studies of Snap Lake kimberlite dike by Gernon et al. (2012) show contamination of the kimberlite magma by the country rock onto which it was emplaced. Gernon et al. (2012) presents six kimberlite lithofacies based on the increasing degrees of serpentinization and carbonate replacement; HK1 (least altered) to HK6 (most altered) (Figure 5.3.1-2).

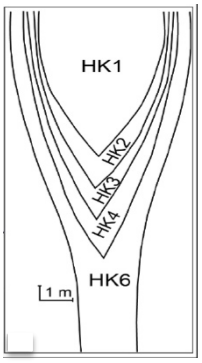

Figure 5.3.1-1 Cross-section profile of the Snap Lake kimberlite showing the kimberlite facies with various degrees of alteration. HK1 (least altered) to HK6 (most altered). (De Beers Internal Report).

Li (2015) studied positive trigons on 14 diamonds from Snap Lake kimberlite using the atomic force microscope (Figure 5.3.1-2).

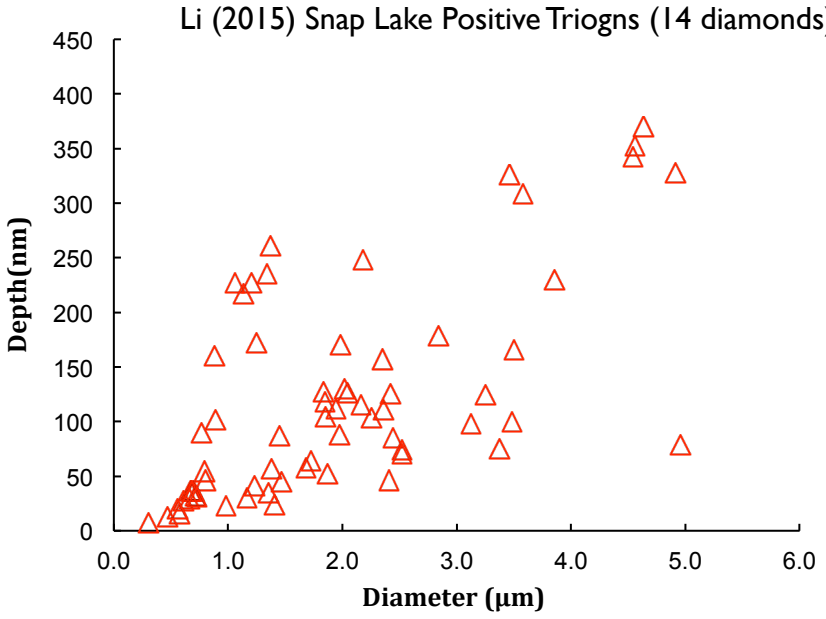

Figure 5.3.1-2 Depth and diameter relationship of positive trigons. Raw data from Li (2015).

Comparing this study's positive trigons sizes to Snap Lake positive trigon sizes will allow for better constraining the conditions of Snap Lake during emplacement. Trigon bottom shape is not considered for the comparison since the bottom shape is dependent on the type of defects present on diamond surface as discussed in chapter **5.2**.

The only resorption experiment with comparable trigon size is at 700 °C in Air after 5 hours (Figure 5.3.1-3).

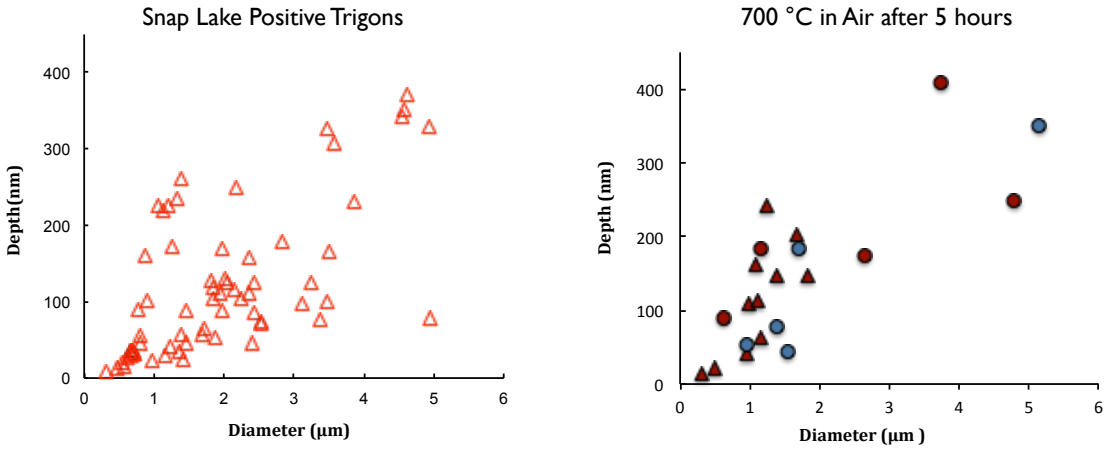

Figure 5.3.1-3 Comparison of Snap Lake positive trigons to resorption experiment at 700 °C in oxygen fugacities of air at atmospheric pressure for 5 hours.

It is possible that Snap Lake diamond resoprtion occurred in a Cl-rich melt/fluid at 700 °C in oxygen fugacities of air at atmospheric pressure for 5 hours.

5.3.3 Extent of near surface diamond resorption

This study confirms that diamond resorption can occur at 700 °C and 800 °C near surface (< 3 km) by interaction between meteoric fluids, which are in equilibrium with the atmosphere and the emplaced kimberlite. At 800 °C in CO_2 atmosphere, diamond resorption occurs and not at 700 °C therefore, a temperature limit of 800 °C is defined for diamond resorption in oxygen fugacities of CO_2. Diamond resorption occurs at 700 °C in oxygen fugacities of air but not in oxygen fugacities of CO_2 therefore, we can conclude that there is a significant oxygen fugacity control on diamond resorption occurring at temperatures < 800 °C. I suggest that diamond resorption at temperatures < 800 °C (at 0.1 MPa) in Cl-rich carbonate kimberlites require strongly oxidized fluids/melts to occur. The temperature limit for diamond resorption in oxygen fugacities of air is still unknown

and should be determined by conducting more experiments.

5.3.4 Conclusions

From overall results, it can be concluded that there is an individual temperature and oxygen fugacity control on positive trigon morphology. Increasing temperature increases the size of positive trigons etched and a positive correlation between depths and diameters can be observed. Slight increase of oxygen fugacity from the air to CO_2 decreases primarily the diameters of flat-bottomed positive trigons and increases the diameters and depths of point-bottomed positive trigons. I propose that the diameter ratio between flat-bottomed to point-bottomed positive trigons on diamonds in nature could have a correlation with the oxygen fugacity prevalent during the consequent diamond resorption. Further studies will have to be conducted to validate my proposal.

This study's resorption experiment in Cl-rich melt/fluid at 700 °C in oxygen fugacities of air at atmospheric pressure for 5 hours produced positive trigons that overlapped Snap Lake positive trigons measured by Li (2015). However the maximum diamond resorption time is still unconstrained therefore, it would be inaccurate to conclude Snap Lake kimberlite's emplacement conditions.

In summary this study concludes the following:

- 700 °C defines the minimum temperature for diamond resorption at oxygen fugacities of CO_2 ($\log fO_2 = -2.79$).
- The higher the temperature in very oxidized diamond resorption conditions the larger the positive trigons formed.
- Changes in oxygen fugacity (from the air to CO_2) at 800 °C increases the diameters and depths of point-bottomed positive trigons.
- Positive trigon size increases as the duration of resorption increases.
- More experiments need to be conducted to constrain the maximum resorption duration to produce positive trigons before implying Snap Lake kimberlite emplacement conditions.

REFERENCES

Angus, J.C., Dyble, T.J., (1975). *Etching models for a {111} diamond surface*: Calculation of trigon slopes. Surface Science, vol. 50, pp. 157-177.

Brey, G. P., Bulatov, V. K., Girnis, A. V., & Lahaye, Y. (2008). Experimental melting of carbonated peridotite at 6–10 GPa. *Journal of Petrology*, *49*(4), 797-821.

Brooker, R., Sparks, A., Kavanagh, R., & Field, S. (2011). The volatile content of hypabyssal kimberlite magmas: Some constraints from experiments on natural rock compositions. *Bulletin of Volcanology, 73*(8), 959-981.

Bureau, Frost, Bolfan-Casanova, Leroy, Esteve, & Cordier. (2016). Diamond growth in mantle fluids. *LITHOS.*

Clement, C. R., Skinner, E. M. W., & Smith, B. S. (1984). Kimberlite redefined. *The Journal of Geology*, *92*(2), 223-228.

Darken, L., & Gurry, R. W. (1945). The system iron-oxygen. I. The wüstite field and related equilibria. *Journal of the American Chemical Society*, *67*(8), 1398-1412.

De Beers Canada Inc. Kimberlite Petrology Unit. n.d. Internal Report. pp. 17–111
Edgar, A. D. (1973). *Experimental petrology: basic principles and techniques*. Oxford University Press.

Fedortchouk, Y., Manghnani, M., Hushur, A., Shiryaev, A., & Nestola, F. (2011). An atomic force microscopy study of diamond dissolution features: The effect of H_2O and CO_2 in the fluid on diamond morphology. *American Mineralogist, 96*(11), 1768-1775.

Fedortchouk, Y., Canil, D., & Semenets, E. (2007). Mechanisms of diamond oxidation and their bearing on the fluid composition in kimberlite magmas. *American Mineralogist, 92*(7), 1200-1212.

Fedortchouk, Y., & Canil, D. (2009). Diamond oxidation at atmospheric pressure: development of surface features and the effect of oxygen fugacity. *European Journal of Mineralogy*, *21*(3), 623-635.

Fedortchouk, Matveev, & Carlson. (2010). H_2O and CO_2 in kimberlitic fluid as recorded by diamonds and olivines in several Ekati Diamond Mine kimberlites, Northwest Territories, Canada. *Earth and Planetary Science Letters, 289*(3), 549-559.

Fedortchouk, Y., & Zhang, Z. (2011). Diamond resorption: link to metasomatic events in the mantle or record of magmatic fluid in kimberlitic magma?. *The Canadian Mineralogist*, *49*(3), 707-719.

Fedortchouk, Y. (2015). Diamond resorption features as a new method for examining conditions of kimberlite emplacement. *Contributions to Mineralogy and Petrology, 170*(4), 1-19.

Field, M. and Scott-Smith, B.H. (1999). Contrasting geology and near surface emplacement of kimberlite pipes in southern Africa and Canada. Proceedings of the 7th International Kimberlite Conference, vol. 1, pp. 214-227.

Frezzotti, M. L., & Touret, J. L. (2014). CO 2, carbonate-rich melts, and brines in the mantle. *Geoscience Frontiers*, *5*(5), 697-710.Gernon, T., Field, M., & Sparks, R. (2012). Geology of the Snap Lake kimberlite intrusion, Northwest Territories, Canada: Field observations and their interpretation. *Journal of the Geological Society, 169*, 1-16.

Gurney, Hildebrand, Carlson, Fedortchouk, & Dyck. (2004). The morphological characteristics of diamonds from the Ekati property, Northwest Territories, Canada. *LITHOS, 77*(1), 21-38.

Howland, R. and Benatar, L. 1993–2000. A Practical Guide to Scanning Probe Microscopy. Thermomicroscopes.

Keltie, E. (2016). *Diamond dissolution in Na_2CO_3, Na_2CO_3-NaCl, and Na_2CO_3-NaF melts at 950ºC and 0.1 MPa* (honors thesis, Dalhousie University, Halifax).

Khokhryakov, A. F., Pal'yanov, Y. N., & Sobolev, N. V. (2001). Evolution of crystal morphology of natural diamond in dissolution processes: experimental data. In *Doklady Earth Sciences* (Vol. 381, pp. 884-888).

Khokhryakov, & Palyanov. (2006). Revealing of dislocations in diamond crystals by the selective etching method. *Journal of Crystal Growth,293*(2), 469-474.

Khokhryakov, A., & Pal'Yanov, Y. (2007). The evolution of diamond morphology in the process of dissolution: Experimental data. *The American Mineralogist, 92*(5-6), 909.

Khokhryakov, A., & Pal'yanov, Y. (2010). Influence of the fluid composition on diamond dissolution forms in carbonate melts. *American Mineralogist, 95*(10), 1508-1514.

Kjarsgaard, B. A. (2007). Kimberlite pipe models: Significance to exploration. In *Proceedings of Exploration* (Vol. 7, pp. 667-677).

Klein-Bendavid, Izraeli, Hauri, & Navon. (2007). Fluid inclusions in diamonds from the Diavik mine, Canada and the evolution of diamond-forming fluids. *Geochimica Et Cosmochimica Acta, 71*(3), 723-744.

Li, Z. (2017). Resorption of Diamonds from Snap Lake and Ekati Mine Kimberlites (Canada) as an Indicator of the Fluid and Emplacement History (unpublished masters thesis). Department of Earth Sciences, Dalhousie University, Halifax, Nova Scotia.

Li, Z., Fedortchouk, Y., Chinn, I., and Fulop, A. 2015. Micromorphology and resorption of diamonds from Snap Lake and Ekati Mine kimberlites (Canada) as an indicator of fluid and emplacement history. Poster session presented at Geological Association of Canada Annual Conference 2015.

Mitchell, R. (1986). *Kimberlites : Mineralogy, geochemistry, and petrology*. New York: Plenum Press.

Nowicki, T., Crawford, B., Dyck, D., Carlson, J., McElroy, R., Oshust, P., & Helmstaedt, H. (2004). The geology of kimberlite pipes of the Ekati property, Northwest Territories, Canada. *LITHOS*, *76*(1), 1-27.

Palyanov, Sokol, Khokhryakov, & Kruk. (2015). Conditions of diamond crystallization in kimberlite melt: Experimental data. *Russian Geology and Geophysics, 56*(1-2), 196-210.

A R Patel. (1968). Etching of trigons on the (111) faces of diamond. *Journal of Physics D: Applied Physics, 1*(11), 1445-1447.

Pervov, V., Somov, A., Korshunov, S., Dulapchii, E., & Félix, J. (2011). The Catoca kimberlite pipe, Republic of Angola: A paleovolcanological model. *Geology of Ore Deposits, 53*(4), 295-308.

Robinson, D. N. (1979). *Surface textures and other features of diamonds*. publisher not identified.

Sato, M. (1971). Electrochemical measurements and control of oxygen fugacity and other gaseous fugacities with solid electrolyte sensors. In *Research techniques for high pressure and high temperature* (pp. 43-99). Springer Berlin Heidelberg.

Scott Smith, B. (2008). Canadian kimberlites: Geological characteristics relevant to emplacement. *Journal of Volcanology and Geothermal Research, 174*(1), 9-19.

Skinner, E. M. W., & Marsh, J. S. (2004). Distinct kimberlite pipe classes with contrasting eruption processes. *Lithos*, *76*(1), 183-200.

Smit, K., Stachel, V., & Stern, T. (2014). Diamonds in the Attawapiskat area of the Superior craton (Canada): Evidence for a major diamond-forming event younger than 1.1 Ga. *Contributions to Mineralogy and Petrology, 167*(1), 1-16.

Smith, E., Kopylova, M., Nowell, G., Pearson, D., & Ryder, J. (2012). Archean mantle fluids preserved in fibrous diamonds from Wawa, Superior craton. *Geology, 40*(12), 1071.

Sokol, A., Khokhryakov, G., & Palyanov, F. (2015). Composition of primary kimberlite magma: Constraints from melting and diamond dissolution experiments. *Contributions to Mineralogy and Petrology,170*(3), 1-18.

Sokol, & Kruk. (2015). Conditions of kimberlite magma generation: Experimental constraints. *Russian Geology and Geophysics, 56*(1-2), 245-259.

Sonin, V., Zhimulev, M., Chepurov, E., & Fedorov, I. (2008). Diamond stability in NaCl and NaF melts at high pressure. *Doklady Earth Sciences, 420*(1), 641-643.

Sonin, V., Zhimulev, M., Chepurov, E., & Pokhilenko, I. (2009). Diamond stability in silicate-halogenide melts at high pressure. *Doklady Earth Sciences, 425*(2), 441-443.

Sparks, R. J., Brown, R. J., Field, M., & Gilbertson, M. (2007). Kimberlite ascent and eruption. Natur*e*, 450(7172), E21. doi:10.1038/nature06435

Stepanov, Shatsky, Zedgenizov, & Sobolev. (2007). Causes of variations in morphology and impurities of diamonds from the Udachnaya Pipe eclogite. *Russian Geology and Geophysics, 48*(9), 758-769.

Tappert, R., & Tappert, Michelle C. (2011). *Diamonds in nature a guide to rough diamonds*. Berlin ; Heidelberg ; New York: Springer.

Veeco, (2010). Multimode 8 with ScanAsyst Instruction Manual. Veeco Instruments, Inc.

Wilson, L., & Head III, J. W. (2007). An integrated model of kimberlite ascent and eruption. Nature, 447(7140), 53-57. doi:10.1038/nature05692

Yaakov Weiss, John Mcneill, D. Graham Pearson, Geoff M. Nowell, & Chris J. Ottley. (2015). Highly saline fluids from a subducting slab as the source for fluid-rich diamonds. *Nature, 524*(7565), 339.

Yamaoka, S., Kanda, H., & Setaka, N. (1980). Etching of diamond octahedrons at high temperatures and pressure with controlled oxygen partial pressure. *Journal of Materials Science, 15*(2), 332-336.

Zhang, Fedortchouk, & Hanley. (2015). Evolution of diamond resorption in a silicic aqueous fluid at 1–3 GPa: Application to kimberlite emplacement and mantle metasomatism. *LITHOS, 227*, 179-193.

Zhang, Z. (2016). Diamond resorption morphology as a fluid proxy in diamond-bearing environments: Constraints from empirical and experimental studies.

Zinchenko, V. (2008). Morphology of diamonds from kimberlite pipes of the Catoca field, Angola. *Geology of Ore Deposits, 50*(8), 806-814.

APPENDIX

EXPERIMENTS AT 700 °C IN AIR

Run	Trigon	Depth (nm)	Diameter (µm)	Wall Angle	Bottom Shape
Initial	Trigon 1	3.99	1.40		flat
	Triogn 2	4.72	2.82		flat
	smallest	1.79	0.45		flat
Run 1	Trigon 3	204.27	1.68	12.40	point
	Triogn 4	148.29	1.39	11.19	point
	Trigon 5a	109.49	0.97	9.59	point
	Trigon 5b	147.02	1.84	18.79	point
	Triogn 6	242.14	1.23	14.90	point
	Trigon 7	63.41	1.17	4.86	point
	Triogn 8	41.37	0.96	3.29	point
	Trigon 9	13.51	0.31	4.93	point
	Triogn 10	161.87	1.09	13.10	point
	Trigon 11	114.55	1.10	9.28	point
	Trigon 12	22.68	0.50	5.17	point
Run 2	Trigon 13	409.11	3.74	8.15	point
	Trigon 14	88.33	0.61	12.10	point
	Trigon 15	183.45	1.69	10.70	flat
	Trigon 16	53.54	0.94	5.83	flat
	smallest	43.47	1.55	3.17	flat
	Trigon 17	174.94	2.63	5.54	point
	Trigon 18	248.30	4.80	3.75	point
	Trigon 19	351.48	5.14	7.08	flat
	Trigon 20	76.28	1.39	5.40	flat
	Trigon 21	184.48	1.16	14.20	point

EXPERIMENTS AT 800 °C IN AIR TRIGON DATA

Run	Trigon	Depth (nm)	Diameter (µm)	Wall Angle	Bottom Shape
Initial	trigon 1	93.39	18.014	0.872	point
	trigon 2	15.437	2.544	0.646	point
Run 1	trigon 3	432.44	4.362	8.031	point
	trigon 4	18.929	0.409	4.4	point
	trigon 5	399.83	6.817	4.5	point
	trigon 6	724.612	5.921	14.8	point
	trigon 7	46.38	0.72	5.518	point
	trigon 8	166.11	3.89	4.942	flat
	trigon 9	68.47	3.938	1.814	flat
Run 2	trigon 10	992	12.089	11.2	point
	trigon 11	301.8	10.272	3.584	flat
	trigon 12	343.087	12.313	3.461	point
	trigon 13	794.203	6.435	11.4	point

EXPERIMENTS AT 800 °C IN CO_2 TRIGON DATA

Run	Trigon	Depth (nm)	Diameter (µm)	Wall Angle	Bottom Shape
Initial	trigon 1	7.56	0.57	1.30	point
	trigon 2	32.88	1.30	2.70	point
	trigon 3	93.86	2.16	3.00	point
	trigon 4	80.02	12.18	0.80	flat
	trigon 4 in	37.11	1.11	3.40	point
Run 1	trigon 5	80.91	12.09	0.80	flat
	trigon 6	99.48	5.79	2.30	flat
	trigon 7	185.11	2.57	10.70	point
	trigon 8	230.11	4.05	5.23	point
	trigon 9	86.26	12.82	1.10	flat
	trigon 10	185.41	7.94	1.50	flat
	trigon 11	143.45	11.82	0.90	flat
	trigon 12	75.40	13.23		flat
	trigon 13	98.20	12.06		flat
	trigon 14	205.05	11.06		flat
	trigon 15	419.58	11.20		flat
	trigon 16	134.91	2.21		point
	trigon 17	52.69	0.99		point